January 2014

Attachment Sites Of Irreversible Cocaine Analogs On The Dopamine Transporter

Rejwi Acharya Dahal

ATTACHMENT SITES OF IRREVERSIBLE COCAINE ANALOGS ON THE
DOPAMINE TRANSPORTER

by

Rejwi Acharya Dahal
Bachelor of Science, East Carolina University, 2007
Master of Science, University of North Carolina – Greensboro, 2009

A Dissertation

Submitted to the Graduate Faculty

Of the

University of North Dakota

In partial fulfillment of the requirements

for a degree of

Doctor of Philosophy
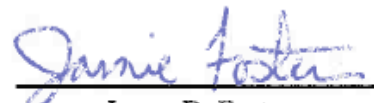
Grand Forks, North Dakota
August
2014
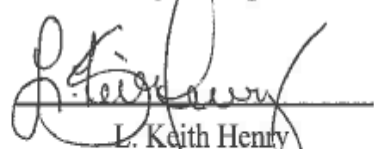
This dissertation, submitted by Rejwi Acharya Dahal in partial fulfillment of the requirements for the Degree of Doctor of Philosophy from the University of North Dakota, has been read by the Faculty Advisory Committee under whom the work has been done and is hereby approved.

Roxanne A. Vaughan

James D. Foster

Joyce Ohm

Brij B. Singh

L. Keith Henry

This dissertation is being submitted by the appointed advisory committee as having met all of the requirements of the School of Graduate Studies at the University of North Dakota and is hereby approved.

Wayne Swisher
Dean of the Graduate School

July 1, 2014
Date

PERMISSION

Title   Attachment Sites Of Irreversible Cocaine Analogs On The Dopamine
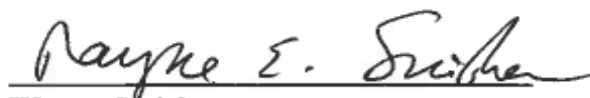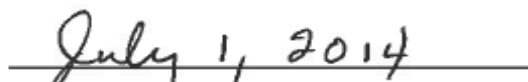Transporter

Department   Biochemistry and Molecular Biology

Degree   Doctor of Philosophy

In presenting this dissertation in partial fulfillment of the requirement for a graduate degree from the University of North Dakota. I agree that the library of this University shall make it freely available for inspection. I further agree that permission for extensive copying for scholarly purposes may be granted by the professor who supervised my dissertation work or, in her absence, by the Chairperson the department or the dean of the School of Graduate Studies. It is understood that any copying or publication or other use of this dissertation or part thereof for financial gain shall not be allowed without my written permission. It is also understood that due recognition shall be given to me and to the University of North Dakota in any scholarly use with may be made of any material in my dissertation.

Signature: Rejwi Acharya Dahal

Date : July 30, 2014

iii

TABLE OF CONTENTS

LIST OF FIGURES

ABBREVIATIONS

5-HT	5-hydroxytryptamine/serotonin
6-OHDA	6-hydroxydopamine
AADC	Amino acid decarboxylase
ADHD	Attention deficit hyperactivity disorder
AMPH	Amphetamine
ANOVA	Analysis of variance
BCA	Bicinchoninic acid
BSA	Bovine serum albumin
CaMKII	Calcium-calmodulin dependent kinase II
CFT	2β-carbomethoxy-3β-(4-fluorophenyl) tropane
CNBr	Cyanogen bromide
DA	Dopamine
DAT	Dopamine transporter
dDAT	Drosophila dopamine transporter
DEEP	1-[2-(diphenylmethoxy)ethyl]-4-2-(4-azido-3-iodophenyl) ethyl piperazine
EL	Extracellular loop
FRET	Fluorescence resonance energy transfer
GA 2-34	N-[n-butyl-4-(4" – azido- 3" – iodophenyl)]-4', 4" – difluoro-3 alpha-(diphenylmethoxy) tropane
GABA	Gamma-aminobutyric acid
GAT	GABA transporter
GBR 12909	1-[2-[bis(4-fluorophenyl)methoxy]ethyl]-4-3-phenylpropyl)piperazine
hDAT	Human dopamine transporter
HVA	Homovanillic acid
IL	Intracellular loop
JHC 2-48	3-(4'-azido-3'-iodo-phenyl)-8-methyl-8-aza-bicyclo-[3.2.1]octane-2-carboxylic acid methyl ester
kDa	Kilodalton
L-DOPA	3,4-dihydroxyphenylalanine
LeuT$_{Aa}$	Leucine transporter from *Aquifex aeolicus*
LLC-PK$_1$ cell	Lewis lung carcinoma porcine kidney cell
MAB	Monoclonal antibody
METH	Methamphetamine
MFZ 2-24	N-[4-(4-azido-3-iodophenyl)butyl]-2-carbomethoxy-3β-(4-clorophenyl)tropane
NE	Norepinephrine
NET	Norepinephrine transporter

NSS	Neurotransmitter: sodium symporter
PCR	Polymerase chain reaction
PD	Parkinson's disease
PICK1	Protein interacting with C-kinase
PKC	Protein kinase C
PP2A	Protein phosphatase 2A
rDAT	Rat dopamine transporter
rGAT1	Rat GABA transporter type 1
RTI 82	3β-(p-chlorophenyl) tropane-2-β-carobxylic acid, 4'-azido-3'-iodophenylethyl ester
SDS-PAGE	Sodium dodecyl sulfate-polyacrylamide gel electrophoresis
SERT	Serotonin transporter
SLC6	Solute carrier family 6
SN	Substantia nigra
TH	Tyrosine hydroxylase
TM	Transmembrane
UV	Ultraviolet
VMAT-2	Vesicular monoamine transporter 2
VTA	Ventral tegmental area

and Dr. Dhasarathy for their guidance and support. I want to thank Dr. Shabb and Wallace for being patient and teaching me about mass spectrometry.

I want to thank my parents for their unconditional love and support. They have always taught me to persevere and that nothing is impossible. "*Udeshya ke lini udi chunu chanda eka*". I want to thank my sister for being my inspiration. I want to thank my in-laws for their blessings. Mostly, I want to thank my husband, who is my rock, for his unconditional love and support. He always listened to me rant about bad days, helped me understand things happen for a reason, for the most part, made fabulous animations for my presentations, went with me to make midnight runs to the lab and sooo sooo much more. It was stressful at times, going through similar hurdles as we were preparing for our defenses together. I am glad we could understand each other's frustrations and happiness. I am so glad we are done and now can start a new journey together. I would not have accomplished all of this without you by my side, my tudka.

To mamu baba

ABSTRACT

The dopamine transporter (DAT) is an integral membrane protein that reuptakes dopamine (DA) from the extracellular space into the presynaptic neuron. DAT regulates dopaminergic neurotransmission as it maintains homeostatic synaptic DA levels in the brain. Psychostimulants such as cocaine disrupt DA homeostasis as it binds to DAT and prevents reuptake of DA. Excess DA in the synapse leads to prolonged dopaminergic neurotransmission, which is associated with cocaine related euphoria often leading to addiction.

The DAT consists of 12 transmembrane domains (TMs) with N- and C-termini facing the cytoplasm. TMs 1, 3, 6, and 8 make up the core of the protein and the residues from these domains are involved in binding substrates and inhibitors. Although the effect of cocaine binding to DAT is known, the mechanism of DAT-cocaine interaction at the molecular level is still unknown. Therefore, to elucidate how cocaine binds to the DAT and how it is positioned in the binding pocket, we mapped the attachment site of the irreversible binding cocaine analogs, $[^{125}I]$MFZ 2-24, $[^{125}I]$RTI 82, and $[^{125}I]$JHC 2-48. These compounds share a similar cocaine-based core structure, but have analog specific photo activatable side chains that extend from different regions of the cocaine core structure. Upon ultraviolet light activation, the photo activatable phenyl N_3 (azido) group forms phenyl nitrene that becomes covalently attached to a residue on the protein, hence irreversible binding cocaine analogs.

Previous studies narrowed the [^{125}I]RTI 82 adduction site to the region surrounding TM6, between Ile291 and Arg344 on human DAT and between Met290 and Lys336 on rat DAT. The [^{125}I]MFZ 2-24 attachment site was localized between residues Ile67 and Leu80 in TM1. To identify the specific amino acid attachment site of these analogs we created several methionine substitution mutants across TMs 1 and 6. This resulted in generation of custom cyanogen bromide (CNBr) cleavage sites. The results from peptide maps of photoaffinity labeled mutants proteolyzed with CNBr narrowed the adduction of [^{125}I]MFZ 2-24 to Asp79 or Leu80 in TM1 and the adduction of [^{125}I]RTI 82 to Phe320 in TM6. Trypsin and CNBr proteolysis of [^{125}I]JHC 2-48 labeled rat DAT indicated a ligand attachment site C-terminal to TM6. Incorporation of three structural analogs to three distinct TM domains demonstrates that the appended azido groups on these analogs identify different faces of the ligand binding pocket. Thus, allowing for triangulation of cocaine orientation in its binding site via computational modeling.

CHAPTER I

INTRODUCTION

Dopamine: Discovery, Synthesis and Degradation

Dopamine (DA) was discovered as a neurotransmitter in 1957 by Dr. Arvid Carlsson (1). Prior to that discovery, DA was thought just to function as a precursor to norepinephrine (1–3). Dopamine governs several physiological roles such as movement, mood, and reward/pleasure. It is considered to be both an inhibitory and an excitatory neurotransmitter depending on synaptic context.

Dopaminergic neurons synthesize DA from tyrosine. Tyrosine is transported into the dopaminergic neurons via amino acid transporters. Once in the neuron, it is converted to DA in a two-step enzymatic process. 1) Cytosolic tyrosine hydroxylase (TH) along with the cofactors oxygen, iron, and tetrahydrobiopterin hydroxylates tyrosine to generate L-3, 4-dihydroxyphenylalanine (L-DOPA), then 2) L-DOPA is decarboxylated to produce dopamine by aromatic L-amino acid decarboxylase (AADC) along with the cofactor pyridoxal phosphate (Figure 1A). The first biosynthesis step catalyzed by TH is the rate limiting step (4). Since DA is the starting compound to generate other neurotransmitters such as norepinephrine and epinephrine, DA synthesis regulates synthesis of other catecholamines.

Figure 1: Biosynthesis and biodegradation of dopamine. Dopamine is synthesized from tyrosine with L-3, 4-dihydroxyphenylalanine (L-DOPA) as an intermediate. Enzymes involved are shown below the arrows. The first catalytic reaction involving tyrosine hydroxylase (TH) is the rate limiting reaction. B) Biodegradation of dopamine. Homovanillic acid (HVA) is the most common product of dopamine degradation in humans.

A

Tyrosine

L-3,4-dihydroxyphenylalanine
(L-DOPA)

Dopamine

Tyrosine
Hydroxylase
(TH)

Aromatic
L-Amino Acid
Decarboxylase
(AADC)

B

Monoamine Oxidase
(MAO)

Catechol-O-methyl-
transferase
(COMT)

Dopamine
(DA)

3,4-Dihydoxyphenlacetaldehyde

Methoxytyramine (MTA)

Aldehyde
dehydrogenase

Monoamine Oxidase
(MAO)

3,4-Dihydoxyphenlacetic acid
(DOPAC)

3-methoxy-4-hydrophenylacetaldehyde

Catechol-O-methyl-
transferase
(COMT)

Aldehyde
dehydrogenase

Homovanillic acid (HVA)

Once synthesized in the body of the neuron, DA molecules are transported toward the nerve terminal and packaged into synaptic vesicles via the vesicular monoamine transporter 2 (VMAT-2), this act helps to prevent oxidative stress in the cytosol (5). The concentration of the neurotransmitter inside the vesicle is 0.1 M, which is 10-100 times higher than in cytosol (4). In addition to the terminal regions, DA synthesis and release also occurs in the dentrites (4).

Upon the arrival of action potential, vesicles storing DA fuse with the membrane and release neurotransmitters into the synapse via calcium (Ca^{+2})-mediated exocytosis. Once in the synapse, DA molecules bind to the pre and post-synaptic dopamine receptors and activate them. This leads to propagation of dopaminergic neurotransmission. Neurotransmission is terminated when excess DA is removed from the synapse. Excess DA in the synapse either diffuses away or is taken back into the pre-synaptic neuron or into the surrounding cells. Once DA is in the presynaptic neuron, it either gets degraded (Figure 1B) or gets repackaged into storage vesicles and awaits the arrival of another nerve stimulation. The amount of dopamine released into the synapse is controlled by the pattern and rate of neuronal firing (6). A schematic diagram of a dopaminergic synapse is depicted in Figure 2.

<u>The Dopaminergic Pathways in the Mammalian Central Nervous System</u>

Soon after the identification of DA as a neurotransmitter, researchers focused to identify the neurons that produce DA. Dopaminergic neurons *in vivo* were identified by fluorescence histochemistry. This technique causes DA to fluoresce when it is combined with a treatment substance, thus lightening up the neurons containing DA (7). Several studies also identified dopaminergic neurons by selecting neurons that contain enzymes

Figure 2: Schematic diagram of a dopaminergic synapse. Once dopamine molecules (orange dots) are synthesized they are packaged into synaptic vesicles (blue circles) via the vesicular monoamine transporter 2 (VMAT-2; purple cylinders). Upon neuron stimulation the synaptic vesicles dock at the plasma membrane and release dopamine into the synapse via Ca^{+2}-mediated exocytosis. Dopamine binds to the post-synaptic receptors (teal cylinders) and initiates dopaminergic neurotransmission (yellow lightening bolts). Dopamine also modulates the autoreceptors (teal cylinders) in the presynaptic neurons. Dopaminergic neurotransmission is terminated when dopamine is removed from the synapse via the dopamine transporter (red trapezoids). Once dopamine is inside the cell it is either repackaged into synaptic vesicles (blue circle) or gets degraded.

Pre-synaptic neuron

Tyr → Tyr → DOPA → DA

Dopamine Autoreceptor

Dopamine Transporter

Dopamine Receptor

Post-synaptic neuron
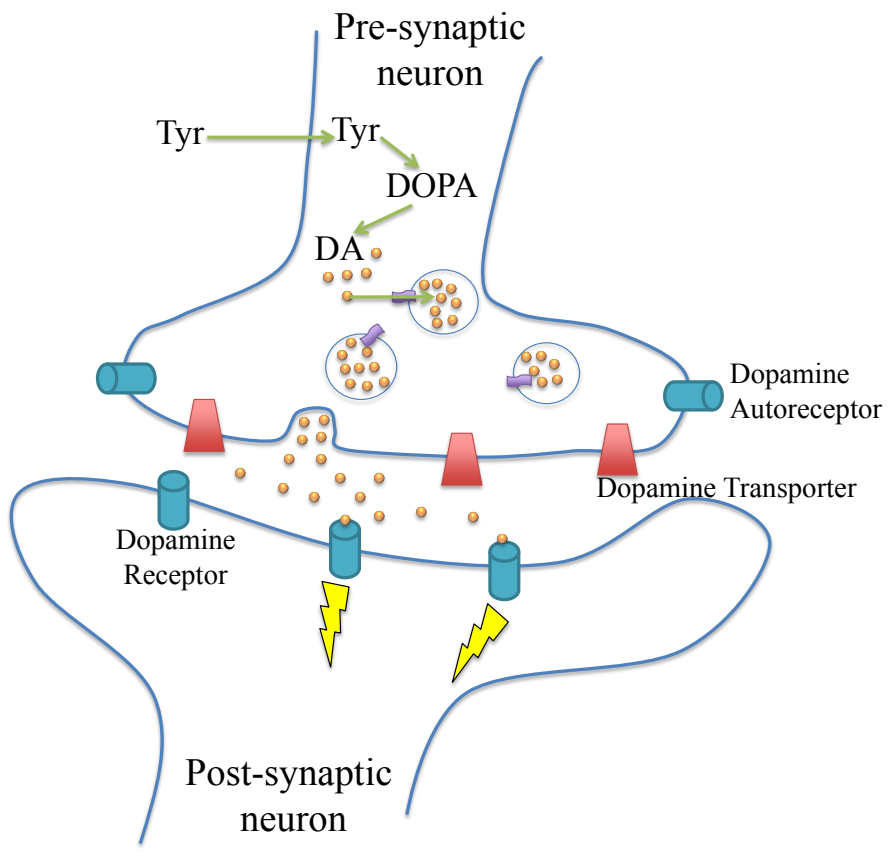
needed for DA biosynthesis (8–10). For example, TH positive neurons were identified as DA-neurons, however, later it was discovered that not all TH positive cells produce DA and therefore are not dopaminergic neurons (11).

Although DA is one of the most abundant catecholamines, dopaminergic neurons account for less than 1% of the total neurons in the body. These neurons are localized in several regions including the retina, the olfactory bulb, mesencephalon, medulla oblongata, and hypothalamus. There are four main dopaminergic pathways in the brain (Figure 3). 1) Nigrostriatal pathway, which extends from the substantia nigra (SN) to striatum in the basal ganglia. These neurons are involved in motor control and movement. 2) Mesolimbic pathway, which projects from the ventral tegmental area (VTA) to the nucleus accumbens. These neurons are involved in the reward and pleasure pathways. 3) Mesocortical pathway, which projects from the VTA to the cortex. These neurons govern motivation, emotion, and attention. 4) Tuberinfundibular pathway, which extends from the hypothalamus to the posterior pituitary. These neurons are involved in inhibition of prolactin secretion. The majority of the dopaminergic neurons are populated in the SN region of the basal ganglia.

Several diseases or disorders occur from dysregulation of these neurons. Dyskinesia and Parkinson's disease result from dysregulation of Nigrostriatal pathway. Schizophrenia and addiction result from dysregulation of Mesolimbic pathway. Attention deficit hyperactivity disorder and depression result from dysregulation of Mesocortical pathway.

Figure 3: Dopaminergic pathways in the human brain. The four major pathways are: Nigrostriatal (red), Mesocortical (blue), Mesolimbic (green), and Tuberinfundibular (pink) pathways.
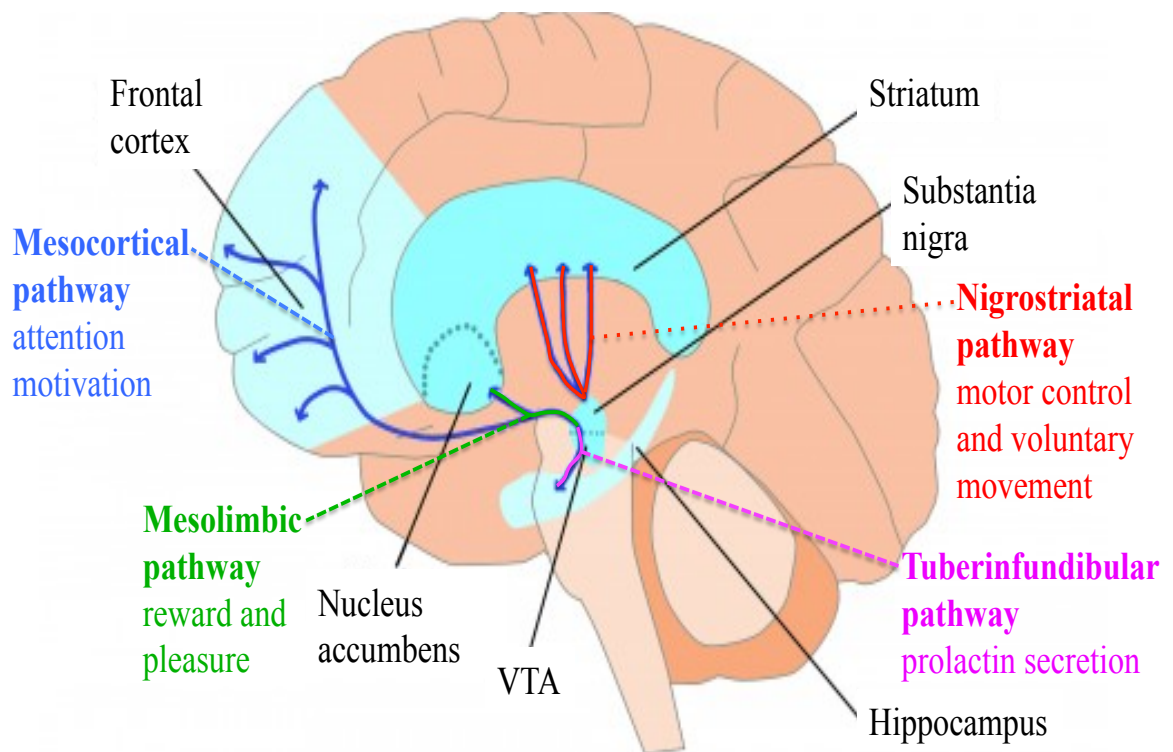
Image modified from Okinawa Institute of Science and Technology (OIST), Okinawa, Japan; with permission

The Dopamine Transporter

Neurotransmitter sodium symporters (NSS) use sodium and chloride electrochemical gradients to drive the reuptake of neurotransmitters such as dopamine, serotonin, and norepinephrine or the reuptake of amino acids such as gamma-aminobutyric acid (GABA) and glycine. These transporters belong to the subfamily solute carrier family 6 (SLC6). In the early 1990s a group of investigators cloned the rat GABA transporter type 1 (rGAT1) encoding gene (12) and hydropathy analysis of GAT and other NSS proteins provided the first structural evidence that these proteins have 12 transmembrane domains with intracellular N- and C-termini (12–14).

The dopamine transporter (DAT) regulates dopaminergic homeostasis by re-uptaking dopamine from the synapse back into the presynaptic neurons. DAT from several species such as rat, human, mouse, monkey, *Drosophila melanogaster*, and *Caenorhabditis elegans* have been cloned. Human (h) DAT and rat (r) DAT sequences have an overall sequence identity of 92%. hDAT and rDAT are composed of 620 and 619 amino acids, respectively, with hDAT containing an extra glycine at position 199 (15). The transmembrane domains are highly conserved between mammalian DAT in regards to the intracellular (IL), extracellular (EL), N- and C-termini. EL2, which connects TM domains 3 and 4, is the largest loop and contains glycosylation sites. Additionally, there are four zinc coordinating sites at positions H193 (EL2), D206 (EL2) H375 (EL4) and E396 (EL4) on hDAT (16, 17). Zinc stabilizes the outward facing conformation of DAT and acts as DA uptake inhibitor.

DAT is regulated by several post-translational modifications such as phosphorylation, palmitoylation, ubiquitylation, and glycosylation (Figure 4).

10

Phosphorylation is a reversible modification in which a phosphate (PO_4^{3-}) group is added to serine, threonine, or tyrosine by a protein kinase. Some key roles of phosphorylation are protein trafficking, protein-protein interaction, and substrate efflux. Threonine 53 and a cluster of serine residues that includes Ser7 in the N- terminal tail on rDAT are a few of the phosphorylation sites (18–22). Proteins are dephosphorylated by protein phosphatases. Another reversible post-translational modification is palmitoylation. It is also a reversible modification where a palmitate group, a 16-chain fatty acid, is added to cysteine residues via a thioester linkage by palmitoyl acyltransferases. This process is reversed by palmitoyl protein thioesterases. Palmitoylation regulates several protein functions including trafficking, stability, and sorting of neuronal proteins (23–25). In regards to DAT, the exact role of palmitoylation is not completely understood. rDAT is palmitoylated at cysteine 580, which is located near the base of TM 12. Other palmitoylation sites are likely to exist but have not been identified yet. Palmitoylation and phosphorylation appear to regulate DAT reciprocally, as palmitoylation helps to stabilize protein on the membrane, and phosphorylation is associated with DAT internalization (26).

Ubiquitylation is a post-translational modification where a ubiquitin group is added to a lysine residue. Protein ubiquitylation governs its interaction with other proteins, its cellular localization, and degradation. In DAT, lysine residues present in the N-terminal tail are the targets for ubiquitylation, which mediates PKC–dependent endocytosis (27, 28). Another post-translation modification DAT undergoes is glycosylation. There are several experimentally determined N-glycosylation sites in EL2 of DAT as denoted by the sequence N-X-S/T. Glycosylation of DAT has been linked to

Figure 4: Schematic diagram of rDAT. The structure contains 12 transmembrane domains with N- and C-termini localized intracellular. Residues in blue represent the residues present in transmembrane domains while residues in tan represent intra- or extracellular residues. Phosphorylation sites discovered thus far are denoted by red circles with "P." Ubiquitylation site are denoted by yellow circles in "Ub." Glycosylation sites and disulfide bond present in EL2 are denoted by green and purple colors, respectively. Palmitoylation site is denoted by orange circle with "Pal."

surface expression which allows DAT to function properly (29–31). Additionally, proper DAT function is also facilitated by proper folding of the protein, which is facilitated by the disulfide bond present in the EL2 between cysteines 180 and 189 (32, 33).

In addition to the post-translational modifications, DAT is also regulated by several proteins that interact with DAT at the N-terminal or C-terminal tails. Syntaxin 1A, protein kinase C (PKC), and protein phosphatase 2A (PP2A$_c$) interact with DAT via the N-terminus while α-synuclein, calcium-dependent calmodulin kinase II (CaMKII) and protein interacting with C kinase-1 (PICK1) interact via the C-terminus (34–36).

DAT: Tertiary Structure

In 2005, the Gouaux laboratory crystalized the leucine transporter from the bacterium *Aquifex aeolicus* (LeuT$_{Aa}$) with the substrate leucine and 2 sodium ions. This provided critical insights into the tertiary structure of homologous transporters such as DAT. LeuT$_{Aa}$ was shown to have a 5+5 helical architecture where TMs 1-5 and 6-10 form helical bundles that are antiparallel, resulting in a pseudo-two-fold axis of symmetry. TMs 1 and 6 contain an unwound region in the middle of the transmembrane that represents non-continuous helices. These two domains along with 3 and 8 form the core of the protein, which contains the substrate-binding site half way into the lipid bilayer (Figure 5). Although the overall sequence identity between LeuT and DAT is only 20%, the residues in the core of the protein surrounding the substrate binding sites are highly conserved with 67% sequence identity, suggesting not only the importance of these residues but also a similar mechanism of transport. TMs 11 and 12 reside on the periphery of the bundle domains. Conserved amino acids throughout the TMs are indicative of their importance in structure-function of the proteins (37, 38).

Figure 5: Schematic 2D representation of DAT based upon LeuT$_{Aa}$ crystal structure. Transmembrane domains 1, 3, 6, and 8 (red cylinders) make the core of the protein. The dopamine binding site is denoted by "S" in a pink hexagon. Purple and green circles represent sodium, and chloride binding sites, respectively.
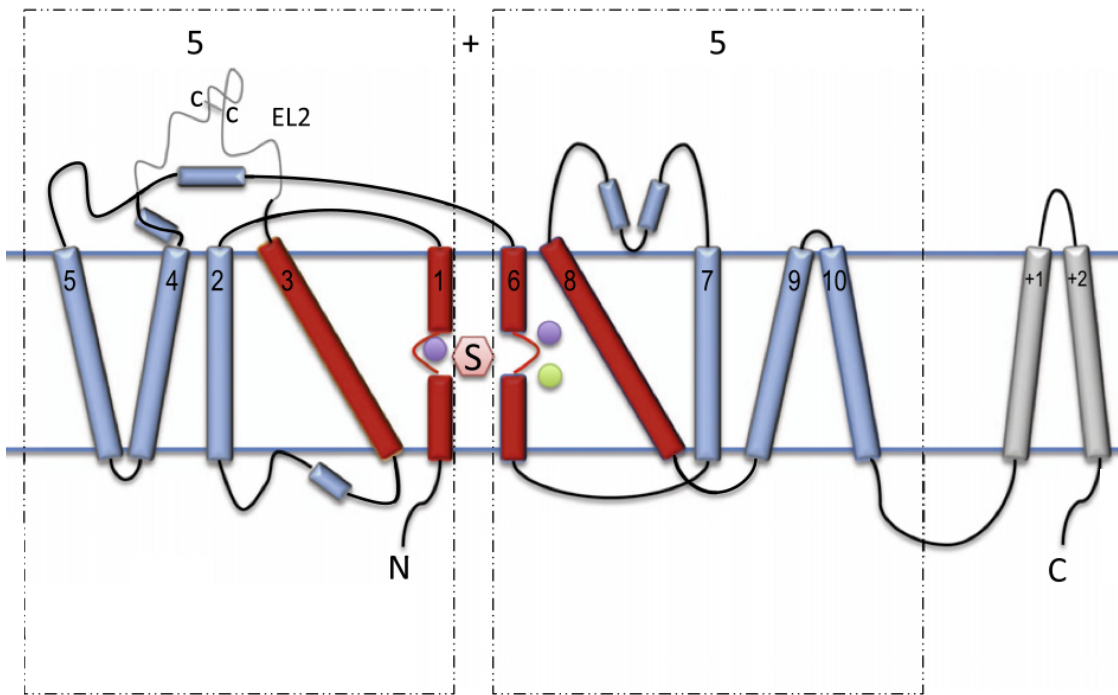
Adapted from Pramod et al. 2012; with permission.

Although LeuT$_{Aa}$ crystal structure showed the binding sites for two sodium ions, it did not identify the binding site for chloride ion, as LeuT$_{Aa}$ does not require chloride to translocate its substrate. However, biochemical studies elucidate the chloride binding site to be near the Na1 binding site (39–42).

There are several differences between the prokaryotic and the eukaryotic SLC6 transporters (37). The eukaryotic transporters have 1) a much longer intracellular N- and C- termini 2) a longer EL2 loop that contains a disulfide bond along with glycosylation sites and 3) several post-translational modifications. Despite these differences, and the fact that LeuT does not bind cocaine, it has been used as a template to build DAT homology models to elucidate the cocaine binding site (43, 44).

DAT: Target of Psychostimulants and Therapeutic Drugs

DAT controls the magnitude and duration of dopaminergic neurotransmission. DA homeostasis is tightly regulated, from its synthesis to its degradation. Several drugs can attribute to dysregulation of DA homeostasis by increasing synaptic DA levels. Consequently, post-synaptic DA receptors become stimulated for prolonged time, which can result into drug associated euphoria, often leading to addiction (45).

Psychostimulants and therapeutic drugs such as cocaine, bupropion (Wellbutrin®, an antidepressant), methylphenidate (Ritalin®, ADHD medication), and mazindol (Mazindor®, an appetite suppressant) are classified as strong DAT inhibitors. These blockers bind to the DAT and inhibit the reuptake on dopamine, which leads to increased synaptic dopamine levels. In contrast, other psychostimulants such as amphetamine and methamphetamine are classified as substrates. These substrates compete with the endogenous substrate, DA, and get transported into the presynaptic neurons through DAT

where they induce efflux of intracellular DA via reverse transport. The mechanisms of actions of cocaine and amphetamine are different; however, the net effect of these drugs is increased synaptic DA levels and prolonged neuron stimulations (46, 47).

<p style="text-align:center;">The Dopamine Hypothesis and Cocaine</p>

Cocaine is a nonselective drug that binds to DAT, SERT and NET and blocks the reuptake of dopamine, serotonin, and norepinephrine, respectively, and thus elevates their levels in the synapse. However, the addictive properties of cocaine are attributed to its ability of elevate DA levels in the nucleus accumbens in the mesolimbic system as stated in the dopamine hypothesis (48).

To test the dopamine hypothesis a DAT knockout (KO) mouse was created by the Caron laboratory in 1996. In this model, DA was cleared from the synapse 100 times slowly than in the WT model, which indicated clearance by diffusion. In the WT model, the faster clearance is due to the presence of DAT, thus, DA transport via DAT is the primary mechanism of terminating DA neurotransmission. Additionally, WT and KO mice injected with cocaine had similar locomotor activity and moreover, cocaine injections did not show additive hyperlocomoter effect in DAT KO mice (49).

However, Rocha et al. showed DAT KO mice self-administered cocaine and additionally, Sora et al. showed these mice display cocaine-conditioned place preference (50, 51). These findings shed a shadow of doubt on the dopamine hypothesis and possibility of other systems, such as serotonergic system, being involved in rewarding effects of cocaine. The DAT KO models show several adaptive changes such as altered DA synthesis, storage, and decreased levels of DA receptors (49). NET and SERT specific inhibitors have displayed conditioned place preference in DAT KO mice but not

in WT DAT (52). This suggests that the adaptive changes in DAT KO model could possibly affect the normal reward pathways.

To evaluate the serotonergic system in reward pathways, SERT KO mice were generated. These models also displayed cocaine-conditioned place preference (51). But, combined DAT/SERT KO mice did not display cocaine-conditioned place preference. On the other hand, NET/SERT KO mice and NET/DAT KO mice display cocaine-conditioned place preference (53). All these studies implicate both dopamine and serotonin systems to explain cocaine reward.

More recently, in 2009, Thomsen et al. used several experimental conditions to evaluate DAT KO and SERT KO mice in regards to cocaine addiction. Their data support the dopamine hypothesis and implicate DAT, while eliminating SERT, in reinforcing effects of cocaine. Discrepancy between studies generated from Rocha et al and Thomsen et al could be due to the strain of mice used (54).

Several adaptive changes seen due to complete knockout of DAT should be eliminated with a knockin of mutant DAT. Chen et al. showed that the triple mutation (L104V/F105C/A109V) in TM domain 2 leads to 70-fold reduction is cocaine inhibition while retaining 50% DA transport activity compared to WT DAT (55). Cocaine-insensitive DAT knockin model displayed abolished cocaine self-administration and cocaine reward. These studies re-establish the dopamine hypothesis and implicate the requirement of functional DAT for cocaine reward (56, 57). Moreover, in humans at least 47% of DAT has to be blocked by cocaine to perceive rewarding effects (58, 59).

DAT: Alternating Access Mechanism

In the late 1950s and the early 1960s, it was proposed that the transporters have two conformations: one that faces the extracellular space and the other that faces the intracellular space. By alternating between the two conformations, transporters transport substrate from the extracellular space to the cytoplasm (60, 61). In 1966, Dr. Oleg Jardetzky coined the term "alternating access mechanism" to describe such phenomena (62). Now it is widely accepted that membrane proteins including SLC6 proteins transport their substrates via the alternative access mechanism (63, 64) (Figure 6).

DAT cycles through outward and inward facing conformations that binds and releases substrates on the opposite sides of the membrane. When in the outward open configuration, the cytoplasmic side is sealed off from the aqueous extracellular environment via the "intracellular gate". In the similar manner, when in the inward open configuration, the extracellular side is sealed off from the aqueous intracellular environment via the "extracellular gate". Based on LeuT structures, the extracellular gate in DAT is proposed to be maintained by Arg85 and Asp477 via a water molecule. Additionally, Tyr156 and Phe320 form aromatic lids that act as a secondary external gate to prevent access to the central substrate-binding site. The intracellular gate is formed by Arg60, Ser334, Tyr335, and Asp436. Additionally, tryptophan 63 stabilizes the intracellular halves of TMs 1 and 6. There are several models that predict how substrates are translocated intracellularly. One model suggests the unwound regions in TM 1 and 6 act as a hinge and move the intracellular halves of these domains out of the way and allow the substrate to move in by opening the intracellular gate (37, 64–66). Another model suggests TMs 1, 2, 6, and 7 form a rigid bundle that rocks back and forth to allow intracellular and extracellular conformation changes (63). It has been determined that

Figure 6: Alternating access mechanism of DAT. A) Empty transporter in an outward farcing configuration. The transporter is facing the extracellular space with open "extracellular gate" and closed "intracellular gate." B) Outward facing occupied transporter. The transporter is facing the extracellular space with open "extracellular gate" and closed "intracellular gate." Ions and dopamine bind to their respective binding sites and that causes conformational change in the transporter leading to the occluded state. C) Occluded configuration. Ions and substrate are in their respective binding sites. Both the "extracellular" and "intracellular" gates are closed. D) Inward facing configuration. The "extracellular" gate remains closed while the "intracellular" gate opens allowing the translocation of ions and dopamine.

A. Empty transporter

B. Outward facing

DA
Na⁺   Na⁺
Cl⁻

C. Occluded

DA
Na⁺   Na⁺
Cl⁻

D. Inward facing

Na⁺   Cl⁻   DA   Na⁺

out

in

22
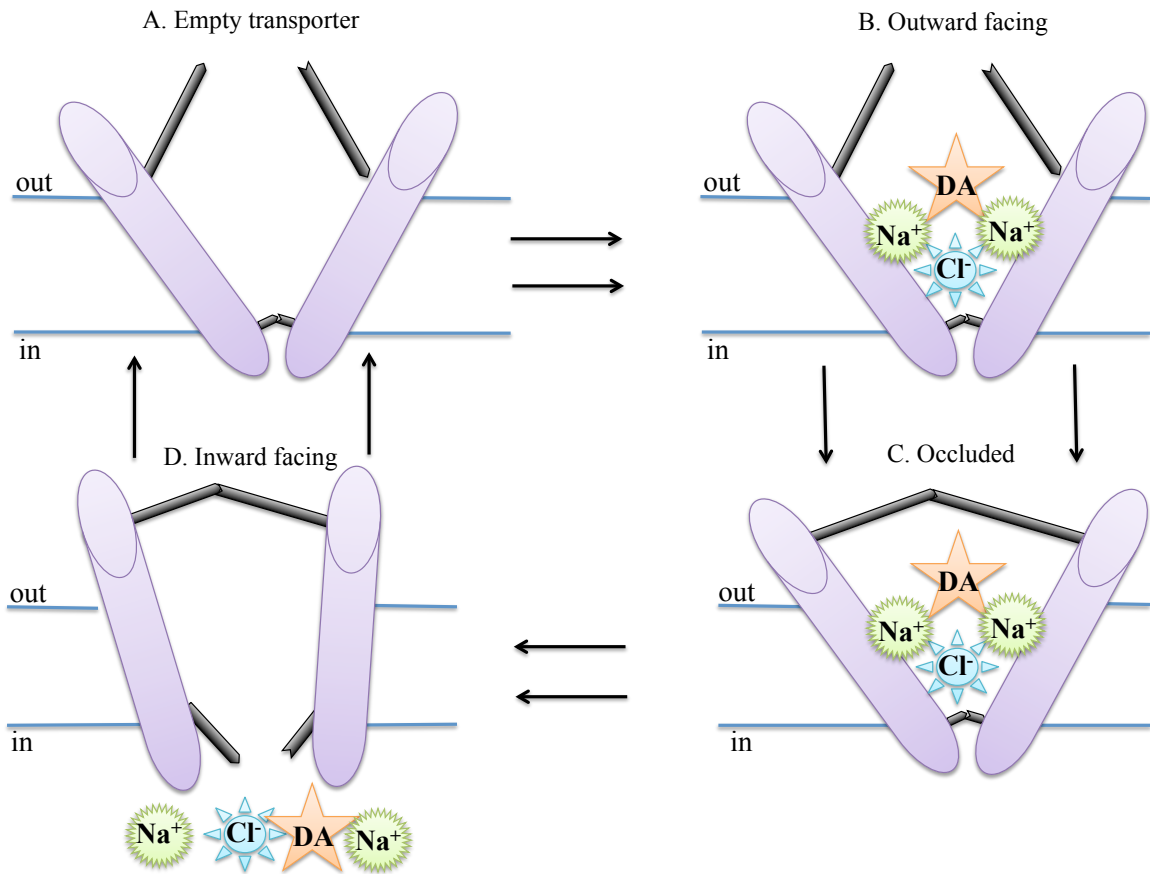
DAT translocates 1DA: $2Na^+$: $1Cl^-$ via alternating access mechanism, even though different models propose different ways of conformational change. Furthermore, DAT also functions as a "channel" where the intracellular and extracellular gates are both open and the transporter lacks the stoichiometric ion movements across the membrane. This "leaking" of substrate is often associated with amphetamine-induced efflux (47, 67).

<u>Dopamine and Inhibitor Binding Sites</u>

Crystal structures of $LeuT_{Aa}$ in various conformations: outward facing, occluded, inward facing and inhibitor-bound forms have provided major insights into structural mechanisms of NSS proteins such as DAT. It was revealed that the substrate-binding site (S1) is composed of residues from TM domains 1, 3, 6, and 8. In fact, mutagenesis of many DAT residues in these TM domains, including Phe76, Asp79, Val152, Phe155, Tyr156, Asn157, Phe319, Val327, and Ser421 reduces dopamine transport (43, 68–76), indicating the involvement of these residues in substrate recognition or translocation. The negative charge of Asp79 in TM domain 1 interacts with the positive charge of DA, which would be present in the cationic form, and aids in binding and transport (68).

Recently, a second substrate-binding site (S2), which is located towards the extracellular vestibule and above the extracellular gate, has been proposed in LeuT. It has been reported that binding of a substrate in the S2 site allosterically modulates the release of ions and substrate from the S1 site and thus aids in substrate translocation. Although the S2 site could be conserved in mammalian NSS transporters, its role and function are still controversial (77, 78).

Just like crystal structures and computational modeling studies based upon the crystal structures have provided insights into the DA binding sites, these studies have also provided insights into the cocaine binding sites. Thus far a crystal structure of a cocaine bound transporter is not available. However, the crystal structures of other inhibitors bound to LeuT has provided insights into the cocaine binding site. Additionally, there are several site-directed mutagenesis, substituted cysteine accessibility method, and quantitative structure activity relationship studies that provide information regarding the cocaine-binding site (79–84). Similar to the interaction between positively charged DA and negatively charged D79, the positively charged tropane nitrogen of cocaine interacts with the negatively charged D79. This salt bridge hypothesis suggests cocaine binds to the S1 site and competitively inhibits DA binding (43, 68). Numerous other residues including Leu104, Phe105, Ala109, Asn157, Tyr251, Tyr273, Thr315 Ser320, Thr455, Ser459 found throughout the core TM domains of DAT have also been implicated in binding of cocaine and its analogs (55, 76, 85). However, with mutagenesis data it is difficult to distinguish between direct effects seen due to involvement of those particular residues with the ligands from indirect effects due to global or macro structural changes. Additionally, mutagenesis could impact electrochemical gradient by disrupting stoichiometric ionic movements and thus also impact DA transport.

Not all DAT inhibitors have the positively charged nitrogen group proposed to interact with D79 (86–88), this suggests the possibility of inhibitors binding differently to the central binding pocket or to sites other than the S1 site. In fact, inhibitor bound LeuT

Figure 7: Putative substrate or inhibitor binding sites. S1 is located in the middle of the transporter half way across the lipid bilayer and below the extracellular gate. S2 is located towards the extracellular vestibule and above the aromatic lid of extracellular gate.
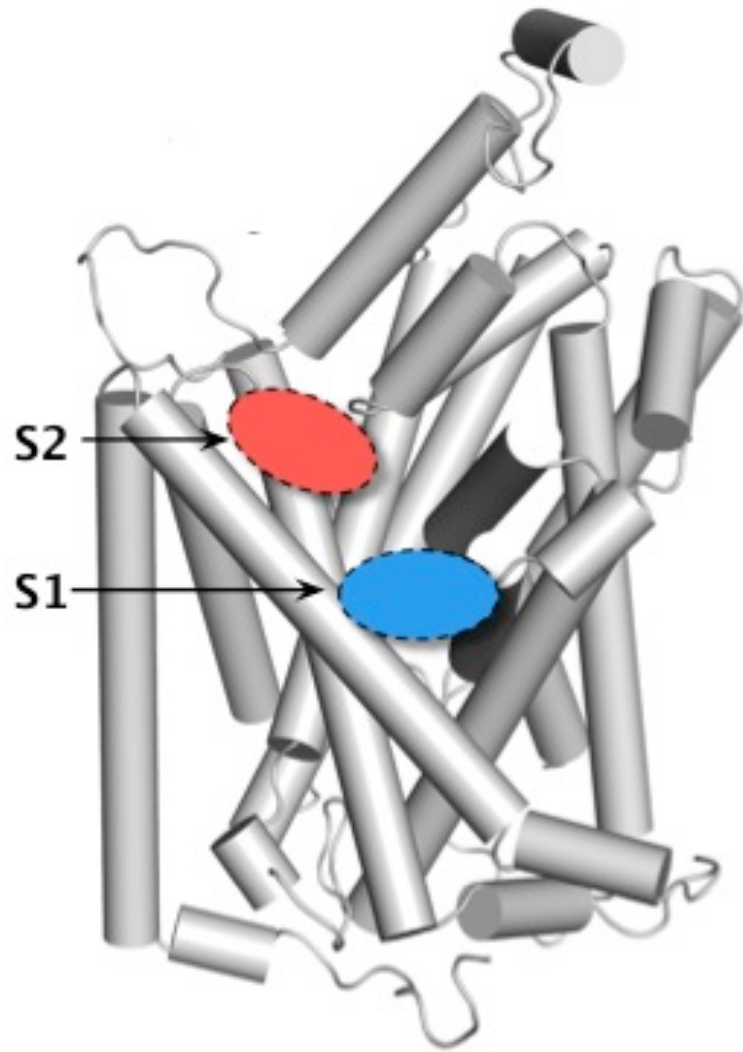
Courtesy of the Henry laboratory, UND.

crystal structures revealed two putative inhibitor binding sites. Figure 7 represents the putative inhibitor/ substrate binding sites. Inhibitors that bind to the S1 site block transport competitively while those that bind to the S2 site block transport non-competitively (65, 89, 90).

Using LeuT as a template, several DAT homology models have been created to investigate the inhibitor binding site, most importantly the cocaine binding site. One such study is by Beuming et al. where several residues were identified to interact with both DA and the cocaine analog, CFT (2β-carbomethoxy-3β-(4-fluorophenyl) tropane). Compared to cocaine, CFT has a higher affinity towards DAT that is attributed to the addition of fluorophenyl moiety at the 3β position of cocaine pharmacophore (Figure 8). Beuming et al. demonstrated the DA binding pocket in DAT is composed of residues from the core domain just as in LeuT. There were several notable key interactions between the protein and the substrate. The protonated amine of DA and the side chain of Asp79 (TM1) form a salt bridge, the catechol ring of DA and Tyr156 (TM3) form aromatic-aromatic staking, and the aromatic ring of DA interacts with Phe76 (TM1), Val152 (TM3), Phe320 (TM6), Phe326 (TM6), Val328 (TM6). Additionally, the unwound regions of TM1 and TM6 were involved in hydrogen bond interaction with DA. Several residues in the middle of TMs 1, 3, 6, and 8 are involved directly or indirectly in coordinating DA (43).

In comparison to DA-DAT interactions, CFT binding involved many of the same residues interactions. Interaction between CFT and DAT residues are depicted in Figure 8B. The protonated amine of CFT forms a polar interaction with the side chain of Asp79 (TM1), the 2β-methylester moiety interacts with Tyr156 (TM3), and the fluoride atom on

the phenylfluoride moiety interacts with nitrogen of Asn157 (TM3). Just as with DA, the tropane ring of CFT interacts with Phe76 (TM1), Val152 (TM3), Phe320 (TM6), Phe326 (TM6), Val328 (TM6). Together these interactions between core residues and CFT indicate the cocaine binding site overlaps with the substrate binding site. The computationally predicted model of CFT bound DAT was experimentally supported by the [^{3}H]CFT binding experiment where the residues shown to interact with CFT were mutated and the [^{3}H]CFT binding of mutant DATs were analyzed and compared to WT DAT (43). Difference between CFT affinity in WT and the mutants indicate involvement of those residues in CFT binding.

Beuming et al. suggested cocaine is a competitive inhibitor and it exerts its inhibition of DA transport by trapping the transporter in the outward facing conformation. This observation is in agreement with studies that have shown increased affinity of cocaine-like compounds in outward open DAT and decreased affinity of cocaine-like compounds in inward open DAT (91–93).

In contrast, the computational docking of cocaine in DAT homology models built by Huang et al. suggest cocaine is a non-competitive inhibitor as it binds to the S2 site (43, 44). Although both Beuming et al. and Huang et al. present experimentally validated poses, the discrepancy in their conclusions suggest the inhibitor binding poses that are predicted by the DAT homology models do not necessarily determine the biologically relevant binding site. Because we lack a crystal structure of cocaine bound NSS transporter and because the computational pose with the lowest energy does not equate biologically stable or preferred pose and cocaine bound, the exact binding site(s) of cocaine on DAT still remain unresolved.

Figure 8: Structures of dopamine, cocaine and cocaine analog- CFT. (Top) Structures of inhibitors and substrate. (Bottom) Computationally predicted and biochemically verified interactions between CFT and DAT residues via backbone (BB) or side chain (SC) based upon Beuming et al 2008.

Dopamine   Cocaine   CFT

Ala77, Ser321, Leu322, Gly323: (BB)

Tyr156 (SC + BB)

Asp79 (SC)
Phe76 (BB)

Asn157 (SC + BB)

Phe76, Phe326,
Val328: (SC)
Phe320 (SC + BB)

Ser149, Gly153, Gly426: (BB)
Val152, Ser422, Ala423: (SC + BB)
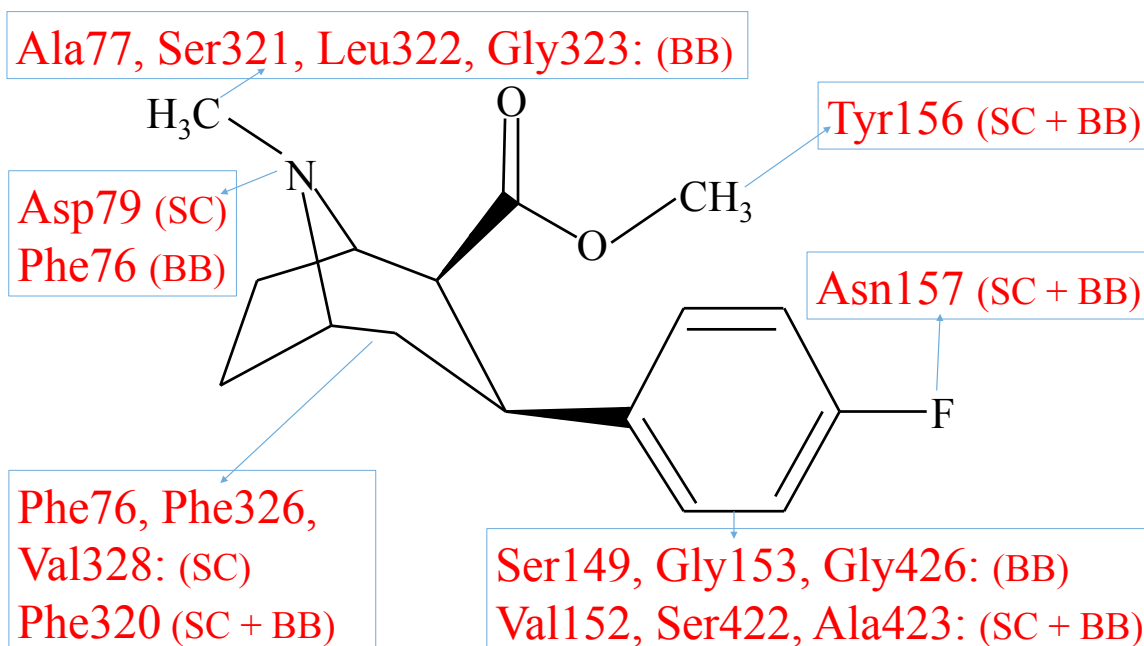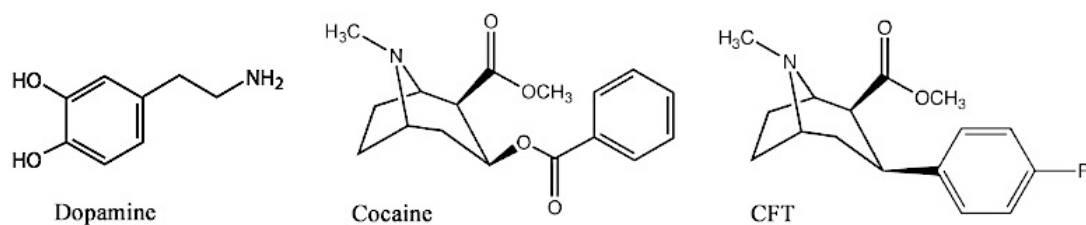
Photoaffinity labeling (PAL) is widely used to identify targets of drugs or to identify a ligand attachment domain. When crystal structures are not available, PAL can be used to determine the three-dimensional orientation of the protein (94, 95). Azido based PALs used in this study contain a photoactivable azido group (N_3) that becomes covalently attached to a residue on a protein when ultraviolent (UV) light induces resonance reorientation in the phenyl ring attached to the N_3 group (Figure 9). Covalent adduction of the ligand occurs via the N group closest to the phenyl ring.

Several structurally different DAT inhibitors such as cocaine, GBR 12909, methylphenidate, bupropion, and benztropine have been used as models to derive diverse PALs which are then used to elucidate the structural properties of DAT. Localization of several DAT PALs analyzed to date are depicted in Figure 10. These analogs bind near TMs 1, 3, 6, and 8, suggesting proximity of these domains in three-dimension. Based upon crystal structures of LeuT$_{Aa}$ and dDAT, it is now known that these domains make up the core of the protein where the substrate-binding site lies.

In this study, we used the combination of tropane-based and non-tropane based irreversible PALs to study DAT structure. The tropane-based irreversible cocaine PALs are [^{125}I]RTI 82 ([^{125}I]3β-(*p*-chlorophenyl)tropane-2β-carboxylic acid, 4′-azido-3′-iodophenylethyl ester), [^{125}I]MFZ 2-24 (N-[4-(4-azido-3-(125)I-iodophenyl)-butyl]-2-beta-carbomethoxy-3beta-(4-chlorophenyl) tropane), and [^{125}I]JHC 2-48(3-(4'-azido-3'-iodo-phenl)-8-methyl-8-aza-bicyclo-[3.2.2]octane-2-carboxylic acid methyl ester) (Figure

Figure 9: Phenyl azido moiety. Movement of electrons in the phenyl ring upon UV light activation leads to formation of nitrene. N^+ and N^- groups are removed as the nitrene group adducts to C-H or N-H groups of a protein via a nucleophilic attack.
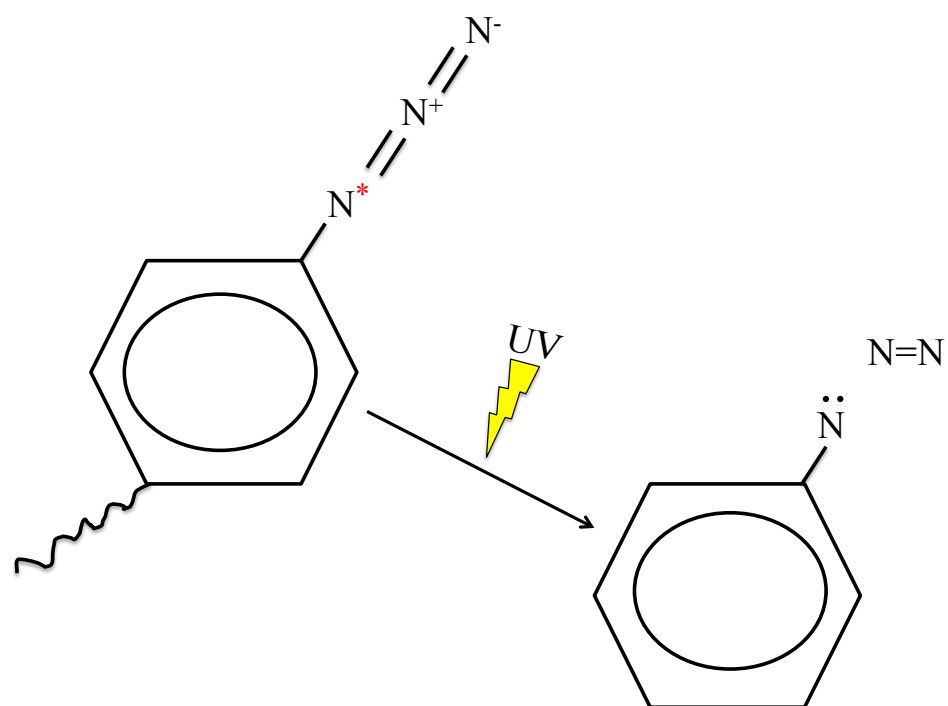
Figure 10: Adduction regions of DAT inhibitors. GBR analogs: [125I]AD 96, and [125I]DEEP; cocaine analog: [125I]MFZ 2-24; and Benztropine analog: [125I]GA 2-34 adduct to TM 1-2. Cocaine Analog: [125I]RTI 82 adducts to TM6. Cocaine analog [125I]JHC 2-48 adducts TM7-12. Grey shaded TM cylinders represent the core domains.

[125I]GA 2-34

[125I]AD 96

[125I]DEEP

| 1 | 2 | 3 | 4 | 5 | 6 | 7 | 8 | 9 | 10 | 11 | 12 |

[125I]MFZ 2-24

[125I]RTI 82
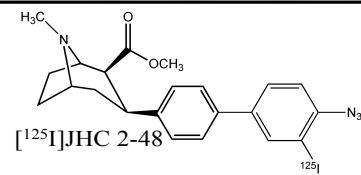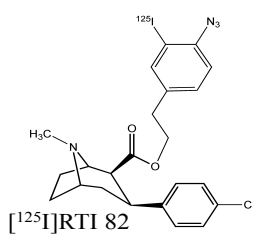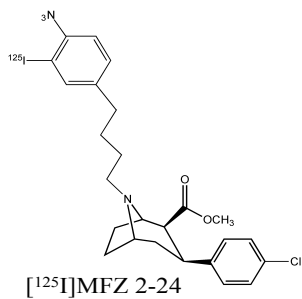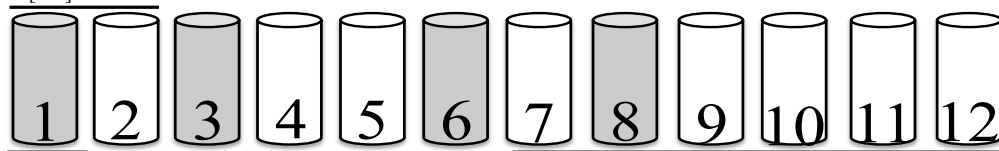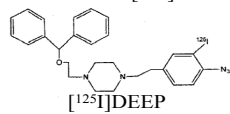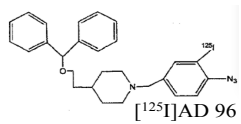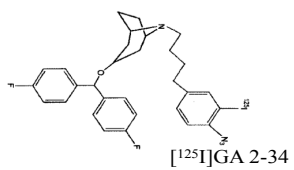
[125I]JHC 2-48

Figure 11: Structures of cocaine and irreversible cocaine analogs, [125I]RTI 82, [125I]MFZ 2-24, and [125I]JHC 2-48. These structurally similar cocaine analogs differ based upon where the phenyl azido group is inserted in the cocaine pharmacophore. In [125I]RTI 82, the phenyl azido group is inserted at the ester moiety. In [125I]MFZ 2-24, the phenyl azido group is inserted at the tropane nitrogen. In [125I]JHC 2-48, the phenyl azido group is inserted at the benzoyl moiety.

Cocaine

[125I]RTI 82

[125I]MFZ 2-24

[125I]JHC 2-48
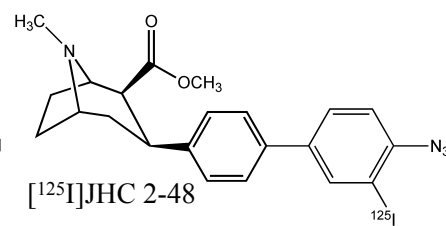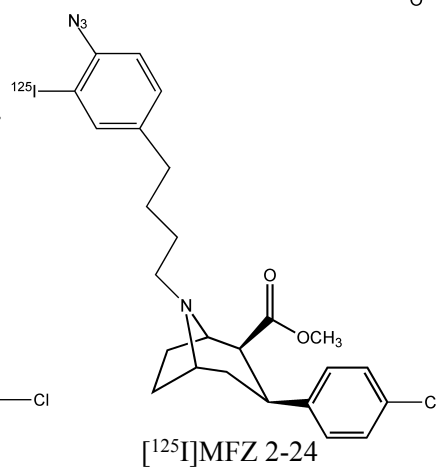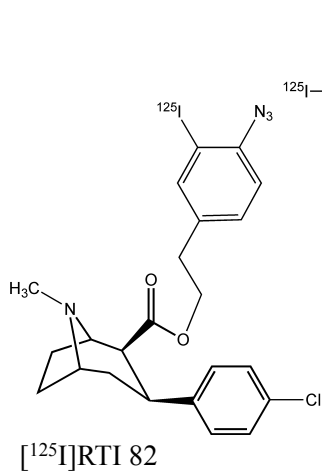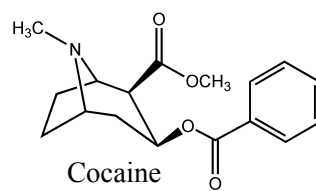
11). These cocaine structural analogs share the main pharmacophore with cocaine in that they all contain the tropane, ester, and benzoyl moieties similar to cocaine. They differ from one another and from cocaine based upon where phenyl azido group is incorporated in the cocaine pharmacophore. In [125I]RTI 82, the phenyl azido group is attached at the ester moiety, in [125I]MFZ 2-24, the phenyl azido group is inserted at the tropane nitrogen and in [125I]JHC 2-48, the phenyl azido group replaces the benzoyl moiety. [125I]RTI 82, [125I]MFZ 2-24, and [125I]JHC 2-48 have affinity towards DAT with K_i of 14.5 nM, 33 ± 4.7 nM, and 15.1± 2.2 nM, respectively (96–99).

Once the PALs are covalently attached to the protein upon UV light activation, DAT is subjected to SDS-PAGE, excised from the gel, and treated with cyanogen bromide (CNBr), which cleaves Met residues at the C-terminal end. The peptide maps generated after chemical proteolysis and epitope specific immunoprecipitation are analyzed to determine the exact incorporation sites of the irreversible analogs. Using irreversible labeling as a strategy for determining the site of ligand-protein interaction, it was previously demonstrated that [125I]RTI 82 cross-links to hDAT within a 40-residue region encompassing TM6 (100) and [125I]MFZ 2-24 cross-links to TM1 between residues 67 and 80 (101), and [125I]JHC 2-48 cross-links C-terminal to TM7, possibly between closely spaced Met residues in TM8 or 12.

In contrast, the non-tropane based PALs are relatively unexplored, thus we evaluated novel methylphenidate based and bupropion based analogs for their ability to label DAT. Methylphenidate (Ritalin®, Concerta®) is used therapeutically to treat ADHD. Ritalin® is an immediate-release drug that is rapidly absorbed while Concerta® has long-acting effects as methylphenidate is slowly released over a period of time.

Bupropion (Wellbutrin®, Zyban®) is widely used as an antidepressant and smoking cessation agent. The neurochemical mechanisms of bupropion are not completely understood. Because of their ability to target DAT with high affinity, these drugs are thought to be a likely target for treatment of cocaine dependency (101,103). Thus, we evaluated a novel azido-iodo-*N*-benzyl derivative of *threo*-methylphenidate analog ($[^{125}I]$RVDU) and a bupropion analog ($[^{125}I]$SADU 3-72) for their ability to label DAT as a first step towards peptide mapping to determine their adduction sites. $[^{125}I]$RVDU has a K_i of 363 nM for $[^3H]$CFT binding and IC_{50} of 2764 nM for $[^3H]$DA uptake (103). Despite the 7-fold decrease in affinity of the analog compared to bupropion (K_i= 3071 nM vs 441 nM), it was bioactive and thus photoaffinity experiments were conducted (104). Our data provide first evidence that these novel compounds target DAT in pharmacological specific manner.

Purpose of the Current Study

The monoamine transporters are implicated in several neurological diseases and disorders including depression, anxiety, addiction, autism spectrum disorder, ADHD, and Parkinson's disease. Both therapeutic and abused drugs are thought to target the transporters and lead to accumulation of dopamine at the synapse. However, not all classes of DAT inhibitors have reinforcing properties, suggesting the mode of blockade could impact different behavioral outcomes: addictive or not. In addition, the tremendous sociological and economical impacts of cocaine addiction make basic understanding of cocaine binding and transport inhibition at the molecular level an important effort for future ventures. Thus, understanding cocaine binding in relation to non-addictive DAT inhibitors could provide critical insights for developing medication strategies toward

treating cocaine addiction. To aid with potential treatments, we are mapping the DAT attachment sites/regions for irreversible cocaine analogs [^{125}I]RTI 82, [^{125}I]MFZ 2-24, and [^{125}I]JHC 2-48. The main differences of these structural analogs, which is the positions of the added phenylazido moiety, are explored to determine the 3 dimensional cocaine orientation in the DAT binding pocket via computational modeling. The phenylazido contact point of these analogs on DAT are distinct and thus, it should provide us with three different contact points, which will be used to triangulate the orientation of cocaine pharmacophore in the binding pocket.

CHAPTER II

MATERIALS AND METHODS

Materials

Reagents

[^{125}I]MFZ 2-24, [^{125}I]RTI 82, and [^{125}I]JHC 2-48 were synthesized by Dr. Amy Newman, Dr. Mu-Fa Zou, Dr. Joo Han Cha, Dr. Comfort Boatang, Ms Jianjian Cao from the National Institute on Drug Abuse. These analogs were radioiodinated by Dr. John Lever as previously described (96–99). Trypsin, trypsin inhibitor, dopamine, (-)-cocaine, mazindol, GBR 12909, nomifensine, desipramine, imipramine, and CNBr were from Sigma-Aldrich (St. Louis, MO). (+)-cocaine was generously provided by Dr. Maarten E. A. Reith (New York University School of Medicine, New York, NY). [^{3}H]2β-carbomethoxy-3β-(4-fluorophenyl) tropane ([^{3}H]CFT) was from Perkin Elmer (Walthman, MA). [^{3}H]Dopamine and high range Rainbow Molecular Markers, and Protein A Sepharose beads were from GE Healthcare Life Sciences (Piscataway, NJ). Lewis Lung Carcinoma Porcine Kidney (LLC-PK$_1$) cells expressing rDAT were kindly provided by Dr. Gary Rudnick (Yale University, New Haven, CT). The QuickChange Mutagenesis kit was from Stratagene (La Jolla, CA). Synthetic oligonucleotide primers were from MWG Operon (Huntsville, AL). Complete Mini Protease inhibitor and FuGENE HD transfection reagents were from Roche Applied Sciences (Indianapolis, IN).

Electrophoresis reagents were from Bio-Rad (Hercules, CA). All other chemicals and reagents were from ThermoFisher (Waltham, MA) or Sigma-Aldrich (St. Louis, MO).

Equipment

Centrifuges

A Beckman Avanti J-25 with 16.250, and 25.50 rotors were used for striatal membrane preparations and harvesting *E. coli* cells for protein and plasmid preparation. Refrigerated Beckman Microfuge R or bench top microfuge 18 were used for general lab procedures under refrigerated or non-refrigerated conditions. A Beckman J6-MI swinging bucket centrifuge was used for cell pelleting, preparing Protein A Sepharose beads, and Protein A cross-linked Sepharose beads.

Electrophoresis, Electroelution, and Dialysis

Sodium dodecyl sulfate poly-acrylamide gel electrophoresis (SDS-PAGE) and protein transfers were performed using a Bio-Rad Mini-Protean III electrophoresis apparatus and the Bio-Rad Mini transblot electrophoresis transfer cell, respectively. Electrophoresis and protein transfer were controlled by Fisher Scientific FB300 power supply. Gels were dried using a Bio-Rad Model 583 gel dryer. Electroelution of proteins was performed using the Bio-Rad Model 422 electroeluter with 3.5 kDa cutoff membrane caps. Electroeluted proteins were dialyzed using ThermoFisher Slide-A-Lyzer® cassettes with 10 kDa cutoff lining.

Spectroscopy

Bicinchoninic acid (BCA) protein assays were quantified using the Molecular Devices SpectraMax 190 plate reader and DNA quantification was performed using Beckman DU640 spectrophotometer. Incorporation of radioactivity during uptake and

binding experiments were counted using a Packard 1900CA or a Beckman LS6500 liquid scintillation counter.

Cell Culture, Molecular Biology, and Miscellaneous

Mammalian cell lines were handled in a sterile Nuair Class II type A/B3 laminar flow hood, and maintained in a Nuair 2700-30 water-jacketed CO_2 incubator. An Eppendorf Mastercycler personal thermocycler was used for all Polymerase Chain Reaction (PCR) experiments. A polytron PT2100 homogenizer was used to homogenize rat striatum membranes. A Thermo Savant SpeecVac® evaporator was used to lyophilize dialyzed and CNBr digested samples. A Fotodyne UV lamp model 3-6000 was used in photoaffinity labeling studies.

Methods

Photoaffnity Labeling- rat striatal membranes

Male and female Sprague Dawley rats (175-300 g) were decapitated and the striatal tissue was immediately removed and weighed. It was placed in ice-cold sucrose-phosphate (SP) buffer (10 mM sodium phosphate, 0.32 M sucrose, pH 7.4) and homogenized with a Plytron Homogenizer in setting 11 for 12-15 sec. Homogenates were centrifuged at 20,000 xg for 12 min at 4 °C followed by two washes with SP buffer and resuspended in Krebs Ringers HEPES (KRH) buffer (25 mM HEPES, 125 mM NaCl, 4.8 mM KCl, 1.2 mM KH_2PO_4, 1.3 mM $CaCl_2$, 1.2 mM $MgSO_4$, 5.6 mM glucose, pH 7.4) to 20 mg/mL original wet weight (O.W.W.). [^{125}I]SADU, [^{125}I]RVDU, and [^{125}I]JHC 2-248 reaction mixtures were prepared in KRH buffer, added to the membranes at various concentration and incubated for 90-120 min at 0 °C to allow equilibration for reversible binding. For cocaine displacement studies, 30 μM of (-)-cocaine was added to the binding

mixture. For pharmacological competition studies, saturating concentrations (1-10 μM) of non-radioactive transporter inhibitors and substrate were added to the binding mixture. Irreversible binding of the photoaffinity analogs to DAT was carried out by directly irradiating the samples with UV lamp (254 nm) for 5 min at a distance of 1 cm. The photolabeled membranes were washed three times with KRH buffer and centrifugation. Samples were resuspended in 100 mM Tris-HCl buffer (pH 8.0) for *in situ* proteolysis or immunoprecipitation (IP) buffer (50 mM Tris-HCl, 0.1% triton X100, pH 8.0) for immunoprecipitation.

Photoaffinity Labeling- rDAT and hDAT expressing cells

Wild type and mutant rDAT and hDAT expressing LLC-PK$_1$ cells were plated on 6-well plates and grown to 90-95% confluency. Growth medium was removed, washed with KRH and incubated with 5 nM raioligand reaction mixtures prepared in KRH buffer for 1.5 – 2 h at 0 °C to allow equilibration for reversible binding. For cocaine displacement studies, 30 μM of (-)-cocaine was added to the binding mixture. The ligands were irreversibly bound onto DAT by direct irradiation with UV (254 nm) light for 5 min at a distance of 1 cm. Photolabeled cells were washed twice with KRH buffer and solubilized with radioimmunoprecipitation assay (RIPA) buffer (1% Triton X-100, 0.1% SDS, 125 mM sodium phosphate, 150 mM NaCl, 2 mM EDTA, 50 mM sodium fluoride, pH 7.4) with Complete Mini protease inhibitor for 30-45 min at 0 °C. Lysates were centrifuged at 20,000 x*g* for 15 min at 4 °C, supernatants were collected and further analyzed.

In situ Trypsin Proteolysis

Photolabeled rat striatal membranes were treated with 10-200 μg/mL of trypsin at 37 °C for 25 min. Equal concentration of trypsin inhibitor was added to the reaction mixture and centrifuged at 20, 000 x*g* for 12 min at 4 °C to quench the reaction. The pellets were solubilized and subjected to immunoprecipitation.

Gel Purification, Electroelution, and Dialysis

Solubilized radiolabeled DATs were subjected to 8% SDS-PAGE. Gels were dried and subjected autoradiography for 12-16 h. The ~80 kDa labeled bands associated with DAT were excised and rehydrated in 1X SDS-PAGE running buffer (25 mM Tris, 192 mM Glycine, and 0.1% SDS). Rehydrated gel pieces were subjected to electroelution at 10 mA/tube for 6 h. Samples were dialyzed against 4 L of MilliQ water for 12-15 h. Radioactivity in samples was assessed by liquid scintillation counting and samples containing equal amounts of radioactivity were lyophilized in a SpeedVac®.

In solution CNBr digestion

Lyophilized samples were incubated with 70% formic acid or with 0.1 mL of 1 M CNBr prepared in 70% formic acid for 24 h at 22 °C. The reactions were quenched by the addition of 900 μL of MilliQ water and lyophilization followed by three washes with MilliQ water and subsequent lyophilization in a SpeedVac® concentrator. The final samples were resuspended in IP buffer and either subjected to IP or acetone precipitation.

Acetone Precipitation

Samples were resuspended in 4SB buffer (50 mM Tris, 5 mM EDTA, 4% SDS, pH 7.4) and acetone in a 1:4 ratio followed by centrifugation at 20,000 x g for 15 min.

Pellets were solubilized in 1X sample buffer and subjected to SDS-PAGE and autoradiography.

Immunoprecipitation, Electrophoresis, Autoradiography, and Western Blot

Solubilized radiolabeled DAT or DAT fragments were subjected to epitope specific immunoprecipitation using antiserum 16 generated against amino acids 42-59 or antiserum C-20 generated against the C-terminal. For cross-linking Ab to protein A sepharose, beads were hydrated and washed three times with triethanolamine (TEA) (0.2 M TEA, pH 8.0). Beads were incubated with polyclonal antibody for 45 min at 22 °C and washed twice with TEA buffer; antibody was cross-linked to the beads by incubation with dimethyl pimelimidate (DMP) for 45 min at 22 °C. The beads were washed twice with 100 mM Tris pH 8.0, rinsed with IP buffer and resuspended and stored in IP buffer containing 0.05% sodium azide. Alternatively, protein A sepharose beads were hydrated and rinsed three times with TEA buffer followed by washes with IP buffer.

Samples were incubated with either beads + antibody or with cross-linked beads for 3 h at 22 °C or alternatively, overnight at 4°C while rotating. Samples and beads were washed four times with IP buffer and eluted with 2X sample buffer. Immunoprecipitated samples were electrophoresed on SDS-PAGE 4-20%, 10-20% or 8% gels followed by autoradiography using Hyperfilm™ MP for 2-8 days at -80 °C. High-range Rainbow Markers were used as molecular mass standards.

For Western blot, proteins were transferred to PVDF membranes following SDS-PAGE. rDAT and hDAT specific primary antibodies were prepared in blocking buffer (3% BSA/ 1% Tween/ 1X PBS) at a 1:1000 ratio. Secondary antibodies were prepared in blocking buffer at 1:5000 ratio. Immunoreactive bands were visualized using Immuno-

Star AP substrate (Bio-Rad) and quantified using a Bio-Rad Chem Doc XRS system and Quantity One 4.6.7 software (Bio-Rad).

[^{3}H]CFT Binding

WT and mutant rDAT and His-hDAT were grown in 24-well plates until 80-90% confluent. Cells were washed twice with 500 μL of ice-cold KRH and incubated with 10 nM [^{3}H]CFT in KRH for 2 h on ice in a final volume of 500 μL. Binding was performed in triplicate with nonspecific binding determined with 15 μM mazindol. The reactions were quenched by washing cells twice with ice-cold KRH followed by solubilization of cells with RIPA buffer containing protease inhibitors. Lysates were assessed for radioactivity by liquid scintillation counting at 52% efficiency and for protein content by the BCA method.

[^{3}H]Dopamine Uptake

WT and mutant rDAT and His-hDAT were grown in 24-well plates until 80-90% confluent. Cells were rinsed twice with 500 μL of 37 °C KRH buffer. Uptake was performed in a final volume of 500 μL KRH with nonspecific uptake determined with 100 μM (–)-cocaine. Assays were initiated by addition of 10 nM [^{3}H]DA plus 3 μM DA and allowed to proceed for 8 min at 37 °C. The reactions were terminated by washing cells twice with ice-cold KRH followed by solubilization of cells with RIPA buffer containing protease inhibitors. Lysates were assessed for radioactivity by liquid scintillation counting and for protein content by the BCA method.

QuickChange® Site-Directed Mutagenesis, Plasmid Transformation, and Transfection

Wild Type (WT) 6xHis-human hDAT in apcDNA 3.1/His and WT rDAT in pcDNA 3.0 were used as starting templates for mutagenesis. Stratagene design primer

software was used to design oligonucleotide primers, which were ordered from MWG operon. QuickChange® method was used to mutant selected residues in order to insert or eliminate CNBr cleavage sites (methionine residues). A 50 µL reaction mixture included 5 µL of 10X reaction buffer (100 mM KCl, 100 mM $(NH_4)_2SO_4$, 200 mM Tris-HCl, 20 mM MgSO4, 1% Triton X-100, 1 mg/mL nuclease free BSA, pH 8.8), 8 µL of Template DNA (5 ng/µL), 1.25-1.60 µL of oligonucleotide forward and reverse primers (125 ng), 2 µL of dNTP mix, 32.5 − 31.8 µL of double distilled DNAse free H_2O. Addition of 1 µL of *pfu Turbo* or *pfu Ultra* DNA Polymerase (2.5 U/µL) initiated the polymerase chain reaction (PCR). PCR cycling parameters included denaturation, annealing, and primer extension. Denaturation required heating the DNA to 95 ºC for 1 min to render it single-stranded. The annealing step was performed at 55 ºC for 1 min and primer extension was done at 68 ºC for 8 min followed by 15 repeated denaturation, annealing, and primer extension cycles. Supercoiled double stranded template DNA was degraded by incubation with 1 µL of DpnI restriction enzyme for 18 h at 37 ºC. The generated plasmid was transformed into Stratagene Giga competent *E coli* cells. 1-4 µL of ligation mixture was added to 25 µL of competent cells. Cells were placed on ice for 5 min and heat shocked for 30 sec at 42 ºC on a heat block. Tubes were placed on ice for 2 min and 250 µL of SOC media was added and cells were plated on carbenicillin resistant agar plates for > 16 h at 37 ºC. The plasmid was isolated using PureYield® Plasmid miniprep System (Promega). DNA was quantified via Epoch microspot spectrometry and sent to verify sequencing to Northwoods DNA (Solway, MN) or MWG operon (Birmingham, AL). LLC-PK$_1$ cells were transfected with His-hDAT and rDAT mutants at 3:2 FuGENE HD to DNA ratio. Cells were selected against G418 and stably expressed DATs. WT and

mutant r/hDAT cells were maintained in a humidified chamber with 5% CO_2 at 37°C in

α-minimum essential medium (AMEM; 5% fetal bovine serum, 2 mM L-glutamine, 200

μg/mL G418, and 100 μg/mL penicillin/streptomycin) for LLC-PK$_1$ cells.

CHAPTER III

RESULTS

Identification of [125I]RTI 82 Adduction Site on hDAT

Previous studies demonstrated that [125I]RTI 82 cross-links to hDAT within a 40-residue region encompassing TM6 (100). Based upon LeuT$_{Aa}$ and dDAT crystal structures, unwound regions in TM domains 1 and 6 accommodate substrate binding and possibly inhibitor binding as well; therefore we started our initial screenings by targeting residues around the unwound region. Additionally, our collaborators (Dr. Henry, Dr. Sharma, and Dr. Akula Bala) computationally predicted two residues near the unwound region, Phe320 and Phe326, as possible sites of adduction. These predictions were made by identifying low energy RTI 82 poses that satisfied the two main biological constraints: interaction between the N$_3$ group and a residue in TM6; and an interaction between the tropane N and the Asp79 side chain. Interaction was defined if the residues were within 5 Å of one another.

We sought to validate the prediction from computational modeling that Phe320 was the likely site of RTI 82 adduction. For this we generated methionine (Met) substitutions of residues flanking Phe320 in hDAT for use in CNBr peptide mapping. To further strengthen the interpretation of the proteolysis patterns, we introduced all TM6 Met substitutions in an M272L background to eliminate Met272 as a CNBr proteolysis

site (100). In hDAT, Met272 is the only Met between TM2 and TM7, thus in the M272L background, the introduction of Mets into TM6 would result in generation of a CNBr fragment of ~50 kDa that would extend from TM2 (Met106, Met111, or Met116) to the inserted Met, or a CNBr fragment of ~6 kDa that would extend from the inserted Met to Met371 in TM7 (Figure 12). The masses of the labeled CNBr fragments produced thus indicate the relative positions of the inserted Mets and the site of [^{125}I]RTI 82 adduction. For ease of discussion, we refer to the double mutants with TM6 Met substitutions in the M272L background solely by the TM6 mutation (e.g. V318M hDAT indicates M272L/V318M hDAT) and to the CNBr fragments by the flanking Mets, although the N-terminus of each fragment is the residue following a proteolyzed Met.

We mutated all residues between V318 and I330 to methionine, except for glycines. Most of the glycine residues examined thus far are shown to be important for DAT activity. Mutations of Gly at positions 323, 325 and 327 either have loss of or greatly reduced plasma membrane expression (105, 106). The mutants generated for this study (V318M, C319M, F320M, S321M, L322M, V324M, F326M, V328M, L329M and I330M) were stably expressed in LLC-PK$_1$ cells and assessed for expression, [^{3}H]DA uptake, [^{3}H]CFT binding, and cocaine displaceable [^{125}I]RTI 82 labeling. Based upon the activities and expression levels, we chose to use V318M, C319M, F320M, S321, L322M, V324M, I330M extensively for peptide mapping studies to identify the [^{125}I]RTI-82 adduction site.

The expression levels determined by immunoblotting of the selected mutants ranged from ~50-100% of WT DAT (Figure 13A), with all showing expression of full length, mature protein. When normalized for transporter expression levels, the mutants

Figure 12: Schematic diagram of hDAT with methionines. A) Schematic diagram of hDAT with endogenous Met residues represented by black dots. Glycosylation sites are represented in extracellular loop 2. B) Cyanogen bromide cleavage at Met in TM5 and TM7 produce an 11 kDa fragment (red shading), which represents the [^{125}I]RTI 82 labeled fragment. C) Strategy for identifying [^{125}I]RTI 82 adduction site. We introduced all TM6 Met substitutions in an M272L background to eliminate Met272 as a CNBr proteolysis site. In hDAT, Met272 is the only Met between TM2 and TM7, thus in the M272L background, the introduction of Mets into TM6 would result in generation of a CNBr fragment of ~50 kDa that would extend from TM2 (Met106, Met111, or Met116) to the inserted Met (blue shaded region), or a CNBr fragment of ~6 kDa that would extend from the inserted Met to Met371 in TM7 (green shaded region).

A

B

C
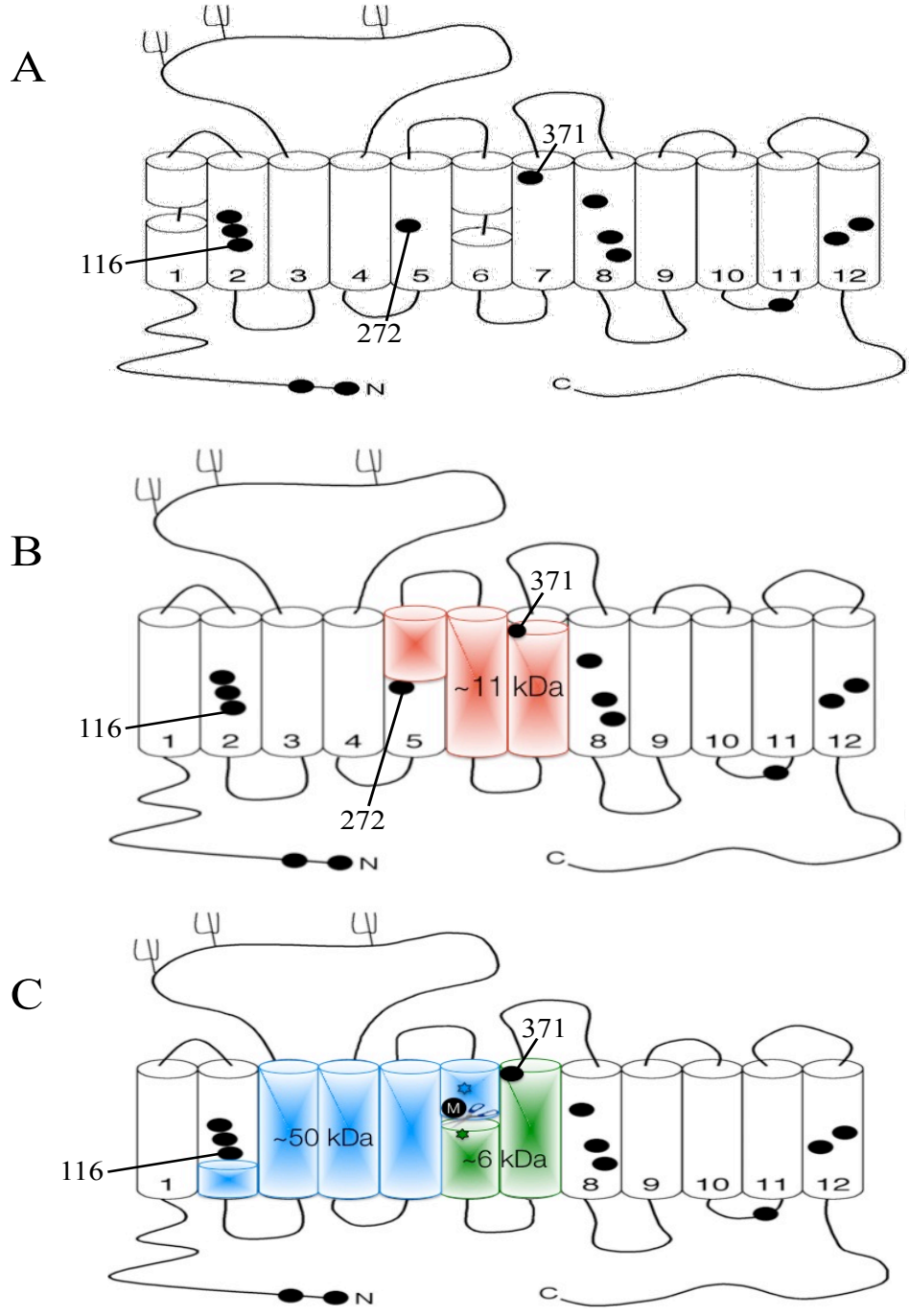
showed [3H]DA uptake values that ranged from ~20-60% of the WT protein, except for F320M and S321M, which exhibited <10% of the WT activity (Figure 13B). Loss of transport in these mutants is consistent with their functional roles, as Phe320 is proposed to act as a substrate pocket gating residue and Ser321 coordinates Na$^+$ at the Na1 site (37, 107). [3H]CFT binding for the mutants was impacted less than transport, ranging from ~60-90% of WT levels when normalized for expression (Figure 13B), and all forms showed [125I]RTI 82 photoaffinity labeling that was fully blocked by cocaine (Figure 13C), indicating that the mutations did not substantially disrupt the cocaine binding pocket.

For peptide mapping studies, the photolabeled proteins were gel purified and subjected to treatment with vehicle (formic acid) or CNBr, followed by SDS-PAGE/autoradiography. Within each experiment, equal amounts of radioactivity for WT and mutant forms were analyzed to allow for direct comparison of peptide fragment production. Figure 14 shows a compilation of representative peptide maps produced from three or more independent replicates for each mutant, with schematic diagrams indicating the primary sequence origin of labeled fragments and site of [125I]RTI 82 adduction (star symbol). Full length, unproteolyzed DAT migrates at ~90 kDa (odd numbered lanes) with no low M_r fragments observed. Aggregates seen at ≥180 kDa are most likely induced by the formic acid treatment, as they were not seen in samples subjected directly to electrophoresis. CNBr treatment of WT hDAT produced a labeled fragment of ~11 kDa (lane 2; arrow a) as we previously demonstrated (100), that corresponds to the region between Met272 and Met371 (calculated mass 10.6 kDa, shaded region in schematic diagram a), as well as larger fragments that likely arise from missed cleavage of Met272.

Figure 13: Characterization of Met-substituted hDATs. (A) LLC-PK$_1$ cells expressing the indicated DAT forms were lysed and equal amounts of protein immunoblotted for DAT. (B) LLC-PK$_1$ cells stably expressing the indicated DAT forms were assayed for [^{3}H]DA uptake (filled bars) or [^{3}H]CFT binding (open bars). Values shown (means of ± S.E.) are normalized for total DAT protein and expressed relative to the WT level (100%). #, $p<0.05$ vs. WT binding; ***, $p<0.001$ vs. WT uptake, by ANOVA with Dunnett's Multiple Comparison Test. (C) Autoradiograph of the indicated hDAT forms photolabeled with [^{125}I]RTI 82 in the presence or absence of 30 μM(–)-cocaine.

A

IB — Mature / Immature

WT V318M C319M F320M S321M L322M V324M I330M

B

[³H]DA Uptake (%WT) / [³H]CFT Binding (%WT)

WT V318M C319M F320M S321M L322M V324M I330M

C

[¹²⁵I]RTI 82

(-) Cocaine   - +   - +   - +   - +   - +   - +   - +   - +

WT V318M C319M F320M S321M L322M V324M I330M
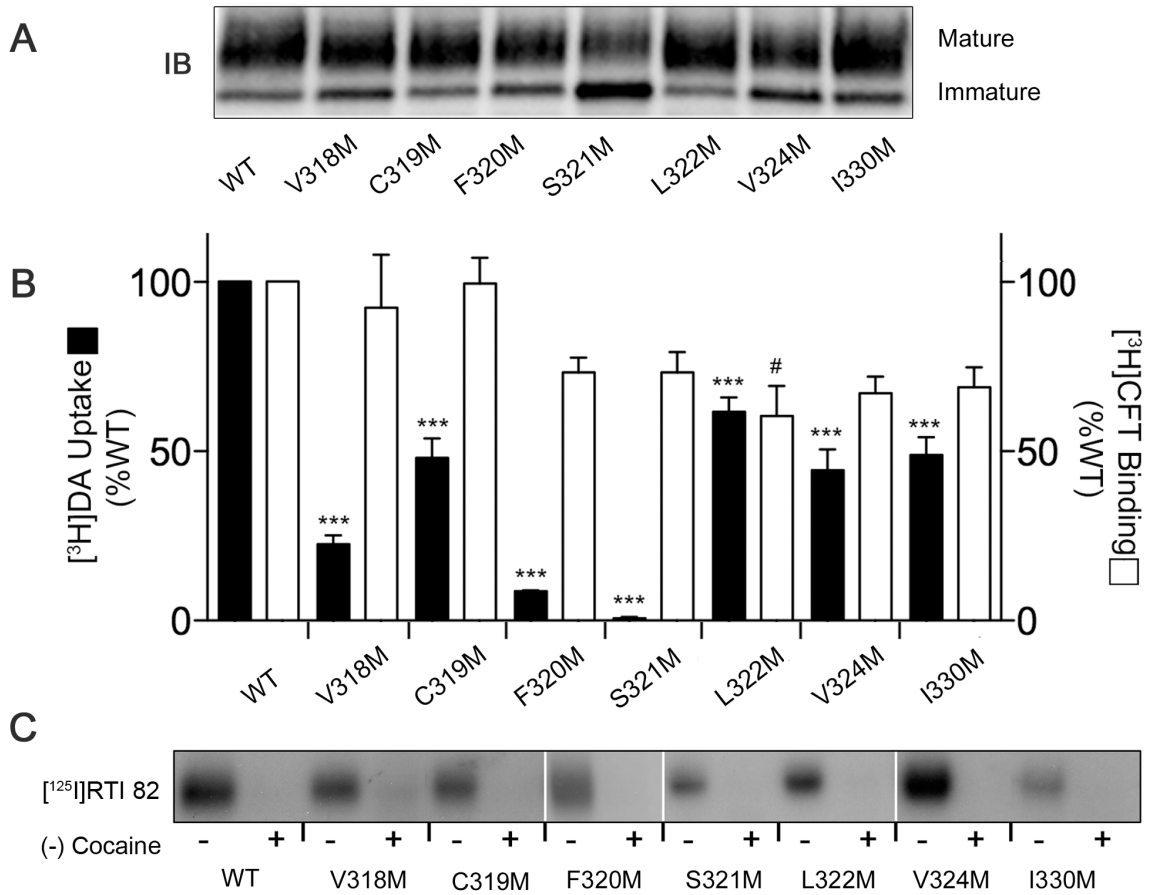
CNBr treatment of [^{125}I]RTI 82-labeled V318M and C319M hDATs produced fragments of ~6 kDa (lanes 4 and 6; arrow b) that are consistent with peptides extending from the inserted Mets to Met371 (calculated masses ~5.6 kDa; shaded region in schematic diagram b), with higher M_r fragments in these samples also indicating missed cleavage of the inserted Mets. In contrast, mutants F320M, S321M, L322M, V324M, and I330M produced only the ~50 kDa fragments (arrow c) that correspond to the shaded region in schematic diagram c (calculated peptide masses ~22.4-23.3 kDa, with additional ~25 kDa of mass contributed from EL2 N-linked carbohydrate), with no production of fragments with masses <8 kDa. These cleavage patterns indicate that ligand adduction occurs C-terminal to V318M and C319M and N-terminal to F320M, S321M, L322M, V324M, and I330M. Because CNBr proteolyzes peptide bonds on the C-terminal side of Mets, the the [^{125}I]RTI 82 adduction site is Phe320. These results also rule out a significant level of [^{125}I]RTI 82 adduction to other residues within this stretch of TM6, including Phe326, an interaction that was suggested by computational modeling.

Although CNBr proteolysis of [^{125}I]RTI 82-labeled F320M, S321M, L322M, V324M, and I330M did not produce the ~6 kDa fragments seen in V318M and C319M hDATs, some lightly labeled fragments of ~8-10 kDa were seen in some digests (Figure 14A). These fragments likely originate from adduction of [^{125}]RTI 82 to a different region of the DAT primary sequence, as we have obtained preliminary evidence from antibody-based mapping that a small fraction of [^{125}I]RTI 82 adduction occurs C-terminal to TM6 (unpublished data). Multi-site incorporation of DAT photoaffinity labels has been previously demonstrated (108), and likely occurs due to the proximity of the TM domains in the protein core in conjunction with small fluctuations in phenylazido moiety

Figure 14: CNBr mapping of [125I]RTI82-labeled TM6 DAT mutants. The indicated DAT forms were photolabeled with [^{125}I]RTI 82 and gel purified. Equal amounts of radioactivity were treated with vehicle (formic acid; odd numbered lanes) or CNBr (even numbered lanes) and analyzed by SDS-PAGE/autoradiography. Unproteolyzed DAT is present in odd numbered lanes at ~90 kDa. CNBr proteolysis of the WT protein produces a fragment of ~11 kDa (lane 2, arrow a) that corresponds to the shaded region in schematic diagram a. CNBr treatment of V318M and C319M hDATs produces fragments of ~6 kDa (lanes 4 and 6, arrow b), that correspond to the shaded region in schematic diagram b. CNBr treatment of the remaining constructs produced fragments of ~50 kDa (lanes 8, 10, 12, 14, and 16, arrow c) that correspond to the shaded region in schematic diagram c, but no fragments of < 8 kDa. The star symbol represents the site of ligand adduction at Phe320. Filled circles in the schematic diagram represent Mets present in the construct.
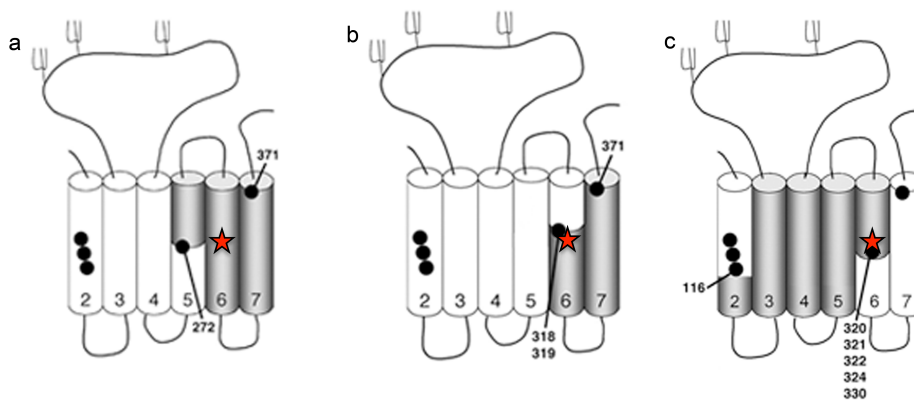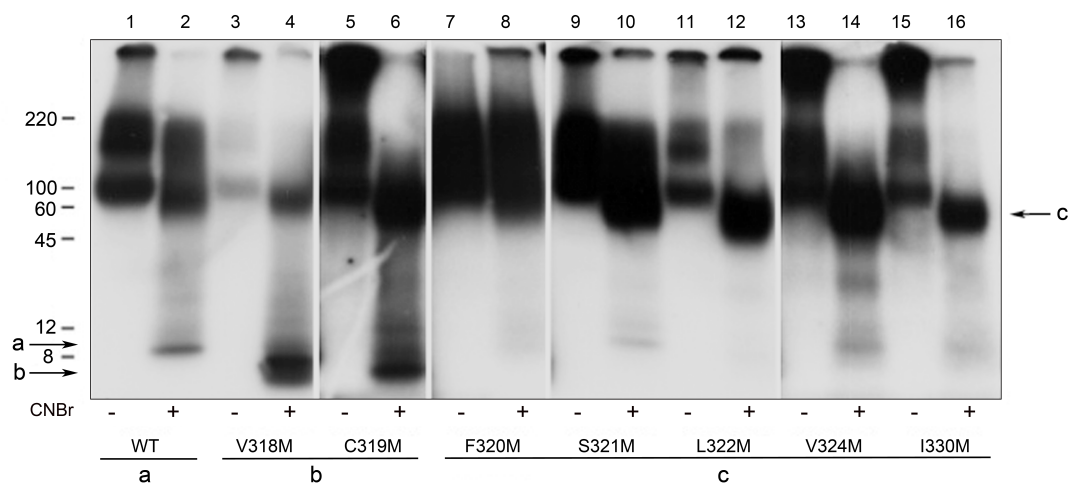
orientation during the photoactivation process. However, the significantly lower labeling intensity of this secondary site relative to that occurring in TM6 indicates that Phe320 is the predominant site of adduction.

<div align="center">

Identification of the [^{125}I]MFZ 2-24 Adduction Site on rDAT

</div>

Previous studies demonstrated that [^{125}I]MFZ 2-24 cross-links to DAT within a 13-residue region in TM1 between Ile67 and Leu80 (101). To further narrow the adduction site, we implemented CNBr peptide mapping analyses with epitope specific immunoprecipitation. In this approach, upon CNBr treatment the inserted Met in TM1 would divide this domain in two halves. Immunoprecipitation of a labeled fragment with Ab16 would indicate adduction is N-terminal to the inserted Met. Likewise, the absence of a photolabeled fragment in the immunoprecipitated sample would indicate adduction is C-terminal to the inserted Met (Figure 15). Therefore, we inserted Met in place of several residues: Leu70, Val73, Ile74, Gly75, Phe76, Ala77, Val78, Asp79, and Leu80, one at a time.

After generating stably expressing rDAT and hDAT mutants in LLC-PK$_1$ cells, we accessed for [^{3}H]DA uptake, [^{3}H]CFT binding, expression level, and cocaine displaceable [^{125}I]MFZ 2-24 labeling. Figure 16 represents an autoradiography of several mutants labeled with [^{125}I]MFZ 2-24 in the presence or absence of cocaine. [^{125}I]MFZ 2-24 labeled cells were lysed, immunoprecipitated with Ab 16 and subjected to autoradiography. [^{125}I]MFZ 2-24 labeling of WT, L80M, V78M, and A77M DATs were displaced by cocaine, however, F76M, G75M, and I74M DAT labeling was not displaced by cocaine and was also weakly labeled compared to the WT. This indicates

Figure 15: Approach to identify the [^{125}I]MFZ 2-24 adduction site. Black dots represent endogenous Mets while black dot with M represents inserted Met. Green bolded line represents epitope for Ab 16. Generation of an immunoprecipitable fragment indicates adduction is N-terminal to the inserted Met (green shaded region). Lack of an immunoprecipitable fragment indicates adduction is C-terminal to the inserted Met (blue shaded region).

Epitope 16
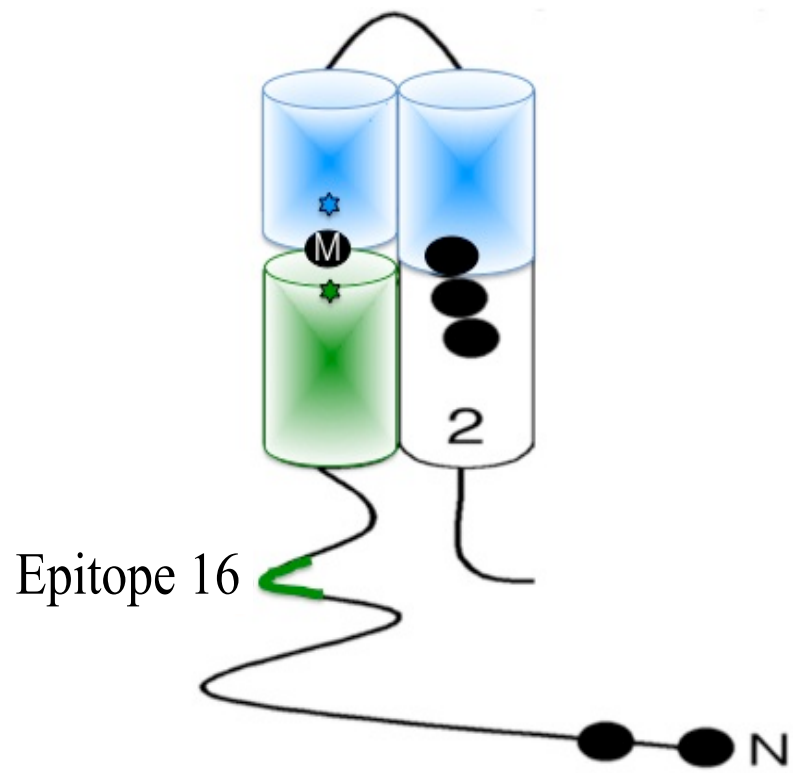
Figure 16: The [^{125}I]MFZ 2-24 photoaffinity labeling of WT and rDAT mutants in the presence or absence of cocaine. Photolabeled DATs were lysed and immunoprecipitated with Ab 16 and subjected to autoradiography. [^{125}I]MFZ 2-24 labeling of WT, L80M, V78M, and A77M is displaced by cocaine. However, [^{125}I]MFZ 2-24 labeling of F76M, G75M, and I74M was not displaced by cocaine and was also weakly labeled compared to the WT.

	WT	L80M	V78M	A77M	F76M	G75M	I74M
(-)-Coc	- +	- +	- +	- +	- +	- +	- +

[^{125}I]MFZ 2-24
rDAT
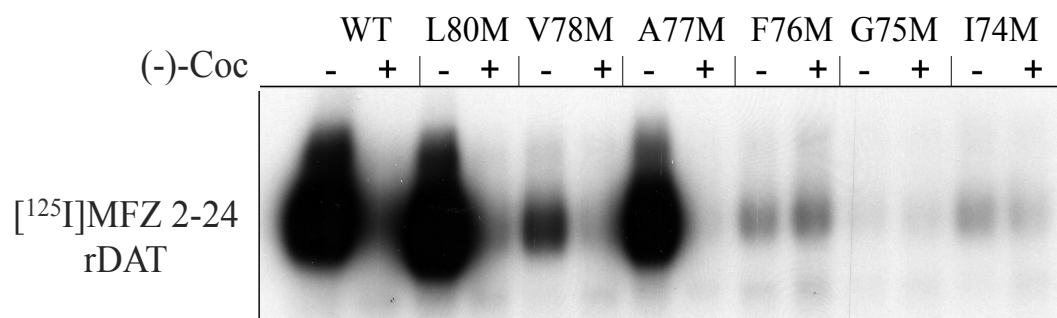
the inserted Met mutations impacted the cocaine binding pocket. Additionally, Phe76 is involved in binding substrate and cocaine (43, 69). Based upon functionality of the mutants, we chose to further analyze L70M, V73M, A77M, V78M and L80M rDATs for peptide mapping.

For peptide mapping studies, the photolabeled proteins were gel purified and subjected to treatment with vehicle (formic acid) or CNBr. Following quenching of CNBr digestion, samples directly subjected to SDS- PAGE/autoradiography are denoted as total while samples immunoprecipitated with Ab 16 prior to SDS- PAGE/autoradiography are denoted as immunoprecipitation. Within each experiment, equal amounts of radioactivity for WT and mutant forms were analyzed to allow for direct comparison of peptide fragment production. Figure 17 shows a compilation of representative peptide maps produced from two or more independent replicates for each mutant, with schematic diagrams indicating the primary sequence origin of labeled fragments and site of [^{125}]MFZ 2-24 adduction (star symbol).

The left panel denotes the fragments generated from CNBr digestion of [^{125}I]MFZ 2-24 labeled WT and mutant DATs. Full length, unproteolyzed DAT migrates at ~90 kDa (odd numbered lanes) with no low M_r fragments observed. Aggregates seen at ≥180 kDa are most likely induced by the formic acid treatment, as they were not seen in samples subjected directly to electrophoresis. CNBr treatment of WT rDAT produced a labeled fragment of ~12kDa (lane 2; arrow a) that was immunoprecipitated with Ab 16 (lane 10) as we previously demonstrated (101). A ~12kDa fragment present in lanes 2 and 10 corresponds to the region between Met1/11 and Met106 (shaded region in left schematic diagram). CNBr treatment of [^{125}I]MFZ 2-24 labeled L80M rDAT produced a fragment

of ~8 kDa, which was also present in IP samples (lanes 4 and 12; arrow b). This is consistent with peptides extending from N-terminus to L80M (shaded region in middle schematic diagram). Additionally, the presence of this fragment is consistent with our previously published data (101). The higher M_r fragments (WT sized fragment) in lane 12 indicate missed cleavage at L80M. This suggests [125I]MFZ 2-24 adduction occurs N-terminal to L80M. Fragments generated by cleavage at V78M and A77M were not immunoprecipitated by Ab 16 (lanes 14 and 16), because cleavage at the inserted Met separated epitope 16 from the adduction site. This indicates the adduction is C-terminal to the inserted Met. Thus, [125I]MFZ 2-24 adduction occurs either at Asp79 or Leu80. Asp79 is a highly conserved essential residue involved in DA transport and as a result its mutation along with mutation of Leu80 have been shown to impact DA binding (43, 68).

Figure 17: CNBr mapping of the [^{125}I]MFZ 2-24-labeled TM1 DAT mutants. The indicated DAT forms were photolabeled with the [^{125}I]MFZ 2-24 and gel purified. Equal amounts of radioactivity were treated with vehicle (formic acid; odd numbered lanes) or CNBr (even numbered lanes) and analyzed by SDS-PAGE autoradiography following immunoprecipitation by Ab 16 when needed. CNBr treatment of WT rDAT produced a labeled fragment of ~12 kDa (lane 2; arrow a) that was immunoprecipitated with Ab 16 (lane 10) (shaded region in left schematic diagram). CNBr treatment of the [^{125}I]MFZ 2-24 labeled L80M rDAT produced fragment of ~8 kDa, which was also present in IP samples (lanes 4 and 12; arrow b) (shaded region in middle schematic diagram). This suggests the [^{125}I]MFZ 2-24 adduction occurs N-terminal to L80M. Fragments generated by cleavage at V78M and A77M were not immunoprecipitated by Ab 16 (lanes 14 and 16), because cleavage at the inserted Met separated epitope 16 from the adduction site. This indicates the adduction is C-terminal to the inserted Met. Thus, the [^{125}I]MFZ 2-24 adduction occurs either at Asp79 or Leu80.
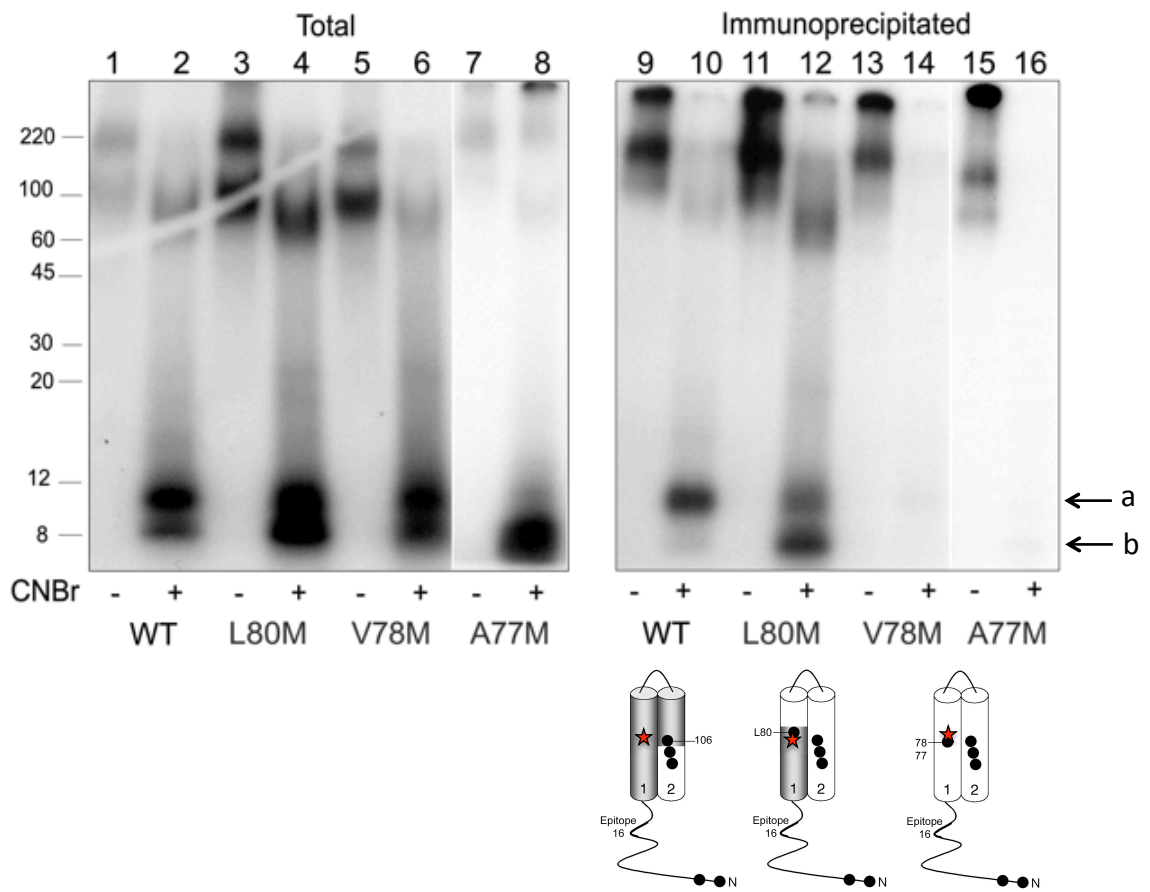
<u>Pharmacological Profile of [^{125}I]JHC 2-48</u>

The third irreversible cocaine PAL we analyzed in this study was [^{125}I]JHC 2-48. This analog is structurally identical to RTI-82 and MFZ 2-24, with an exception of phenylazido positioning on the cocaine pharmacophore. This analog has not been thoroughly investigated, thus, we started our evaluation by determining its pharmacological specificity towards DAT. His-hDAT expressing LLCPK$_1$ cells were labeled with the analog and incubated in the absence or presence of several known DAT inhibitors and the physiological substrate, DA, along with NET and SERT inhibitors (Figure 18). Cells lysates were immunoprecipitated with anti-His antibody to isolate hDAT. Various DAT inhibitors (-)-cocaine, mazindol, GBR 12909, and nomifensine were able to displace [^{125}I]JHC 2-48 labeling of hDAT. Additionally, the endogenous substrate, DA, also displaced [^{125}I]JHC 2-48 labeling of hDAT. However, (+)-cocaine, NET inhibitor desipramine and SERT inhibitor imipramine were unable to displace [^{125}I]JHC 2-48 labeling of hDAT. These results demonstrate pharmacological specificity of [^{125}I]JHC 2-48 towards DAT.

<u>Trypsin Digestion and Epitope Specific Immunoprecipitation of [^{125}I]JHC 2-48 Labeled DAT</u>

CNBr digestion of [^{125}I]JHC 2-48 labeled WT DAT produced a fragment that was not visible in SDS-PAGE. Lack of a fragment indicated the adduction of [^{125}I]JHC 2-48 most likely occurs between the two closely spaced Met residues possibly in TM8 or 12 thus, the generated fragment would be too small to detect by SDS-PAGE. However, recent analyses of [^{125}I]JHC 2-48 labeled WT DAT cleaved with CNBr generated a ~9

Figure 18: Pharmacological profile of hDAT labeled with [^{125}I]JHC 2-48. His-hDAT expressing cells were labeled with [^{125}I]JHC 2-48 in the presence and absence of DAT, NET and SERT inhibitors along with endogenous substrate DA. Cells were lysed, immunoprecipitated with anti-His antibody and subjected to autoradiography. [^{125}I]JHC 2-48 labeling of hDAT was displaced by DAT inhibitors (-)-cocaine, mazindol, GBR 12909, and nomifensine. Additionally, the endogenous substrate, DA, also displaced [^{125}I]JHC 2-48 labeling of hDAT. However, an inactive isomer of cocaine ((+)-cocaine), NET inhibitor desipramine and SERT inhibitor imipramine were unable to displace [^{125}I]JHC 2-48 labeling of hDAT. This represents pharmacological specificity of [^{125}I]JHC 2-48 towards DAT.

Control   (-)-Cocaine   (+)-Cocaine   Mazindol   GBR 12909   Nomifensine   Desipramine   Imipramine   Dopamine
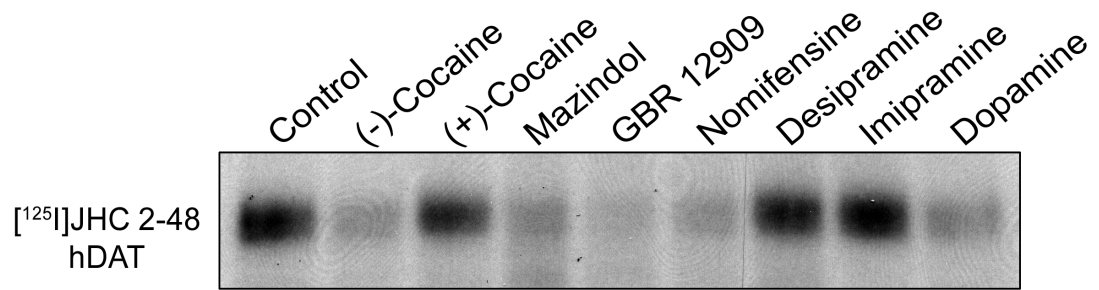
[^{125}I]JHC 2-48
hDAT

kDa fragment. This data indicates our previous hypothesis is not valid. Thus, we analyzed trypsin digestion and epitope specific immunoprecipitation of [^{125}I]JHC 2-48 labeled rat striatal membrane.

Trypsin cleaves at positively charged Lys and Arg; specifically, Arg218 on DAT is readily accessible for trypsin cleavage, which divides photolabeled DAT into two halves. Immunoprecipitation of a ~45 kDa photolabeled fragment by the N-terminal Ab would indicate adduction of the analog occurs N-terminal to Arg218, in TMs 1-3. A ~45 kDa fragment incorporates all residues N-terminal to Arg218, which accounts for ~20 kDa fragment, and glycosylation in EL2, which adds ~ 25 kDa mass to the fragment. However, immunoprecipitation of a ~32 kDa fragment by a C-terminal specific Ab would indicate adduction of the analog occurs C-terminal to Arg218, in TMs 4-12 (109) (Figure 19).

Trypsin digestion and epitope specific immunoprecipitation allows us to determine a broad region where the ligand adducts, thus, rat striatal membranes labeled with [^{125}I]JHC 2-48 were subjected to trypsin digestion and epitope specific immunoprecipitation to determine the region of [^{125}I]JHC 2-48 incorporation. Figure 20 represents trypsin peptide map of [^{125}I]JHC 2-48 labeled rDAT. N-terminal Ab did not immunoprecipitate a photolabeled fragment, which suggests adduction does not occur in TMs 1-3. Presence of ~12 kDa fragment in the C-terminal Ab immunoprecipitated sample of trypsin digested DAT indicates adduction occurs within 12 kDa of the epitope C-20. Trypsin cleavage at a cut site in IL5 would result in a production of ~12 kDa fragment. Thus, this indicates [^{125}I]JHC 2-48 adducts in TM 11-12. However, we cannot rule out the possibility of [^{125}I]JHC 2-48 adduction to TMs 4-10, since there are several

Figure 19: rDAT sequence with trypsin cleavage site at Arg218. Immunoprecipitation of a ~45 kDa photolabeled fragment (yellow) by the N-terminal specific antibody (epitope 16 region; represented by green shaded residues) indicates adduction of the analog occurs N-terminal to Arg218, in TMs 1-3. A ~45 kDa fragment incorporates all residues N-terminal to Arg218, which account for ~20 kDa fragment, and glycosylation in EL2, which adds ~25 kDa mass to the fragment. Immunoprecipitation of a ~32 kDa fragment (blue) by a C-terminal specific antibody (epitope C-20 region; represented by pink shaded residues) indicates adduction of the analog occurs C-terminal to Arg218, in TMs 4-12.

Epitope 16

Epitope C-20
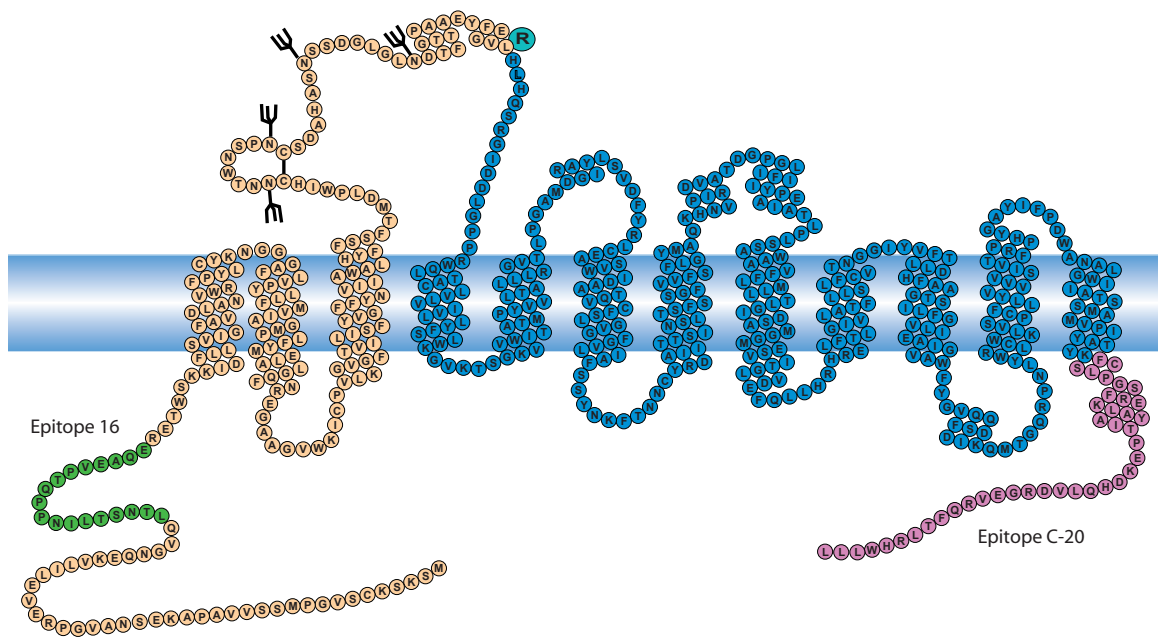
Figure 20: Trypsin digestion and epitope specific immunoprecipitation of [^{125}I]JHC 2-48 labeled rat striatal DAT. Lack of a small M_r photolabeled fragment in the N-terminal Ab pull down lane (2nd lane), indicates adduction does not occur in TMs 1-3. The presence of a ~12 kDa fragment in the C-terminal Ab immunoprecipitated sample of trypsin digested DAT (4th lane) indicates adduction occurs within 12 kDa of the epitope C-20. Trypsin cleavage at either cut site in IL5 would result in a production of a ~12 kDa fragment. Thus, this indicates [^{125}I]JHC 2-48 likely adducts in TM 11-12

Trypsin   -   +   -   +

100 —
60 —

20 —
12 —

8 —

N-Term Ab 16   C-Term Ab 20

Epitope
16

N

C
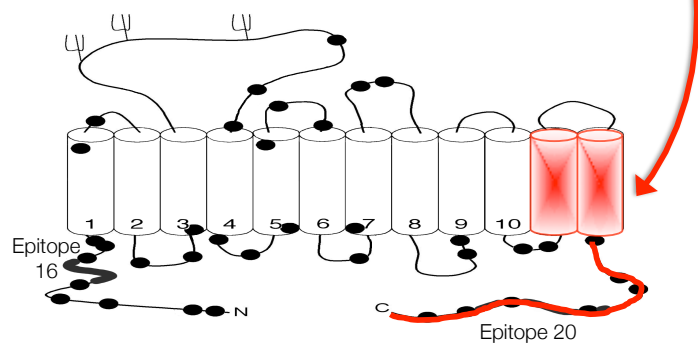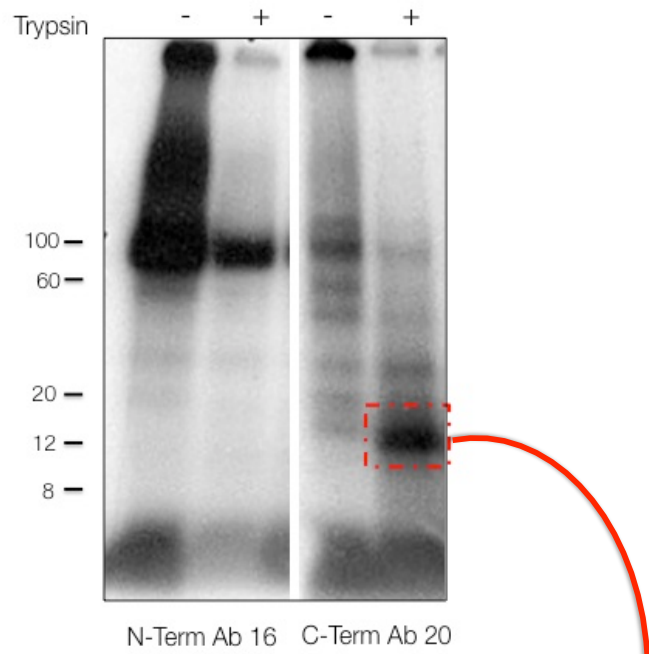
Epitope 20

trypsin cleavage sites present all across DAT and cleavage at those sites would separate the adduction site from the epitope region.

<u>Photoaffinity Labeling of DAT With Methylphenidate Analog ([^{125}I]RVDU)</u>

Methylphenidate is a DAT blocker used therapeutically to treat ADHD. Thus far, its binding site on DAT is not determined. Additionally, non-tropane based PALs are relatively unexplored, thus, we analyzed a novel methylphenidate analog [^{125}I]RVDU to determine its specificity towards DAT as a initial step towards peptide mapping.

Rat striatal membranes were labeled with 30 nM of [^{125}I]RVDU in the presence and absence of 10 mM or 100 mM of β-CFT and D-MPH (Figure 21). Labeled proteins were immunoprecipitated with DAT specific Ab and subjected autoradiography. Labeling of DAT with [^{125}I]RVDU was set at 100%. Incorporation of the ligand was reduced by both β-CFT and D-MPH by 75-90% in a dose dependent manner. This indicates pharmacological specificity of [^{125}I]RVDU for DAT. Most importantly, this is the first successful example of a DAT PAL based on a MPH scaffold (103).

Figure 21: Photoaffinity labeling of DAT with [^{125}I]RVDU. Structures of MPH and RVDU are depicted on top. Rat striatal membranes were photoaffinity labeled with 30 nM [^{125}I]RVDU in the absence or presence of 10 µM or 100 µM β-CFT or D-MPH. Membranes were solubilized and DATs were immunoprecipitated followed by SDS-PAGE and autoradiography. The relevant portion of a representative autoradiograph is pictured followed by a histogram that quantifies relative band intensities. Mean ± SE of three independent experiments is shown; ***$p < 0.001$ versus control.
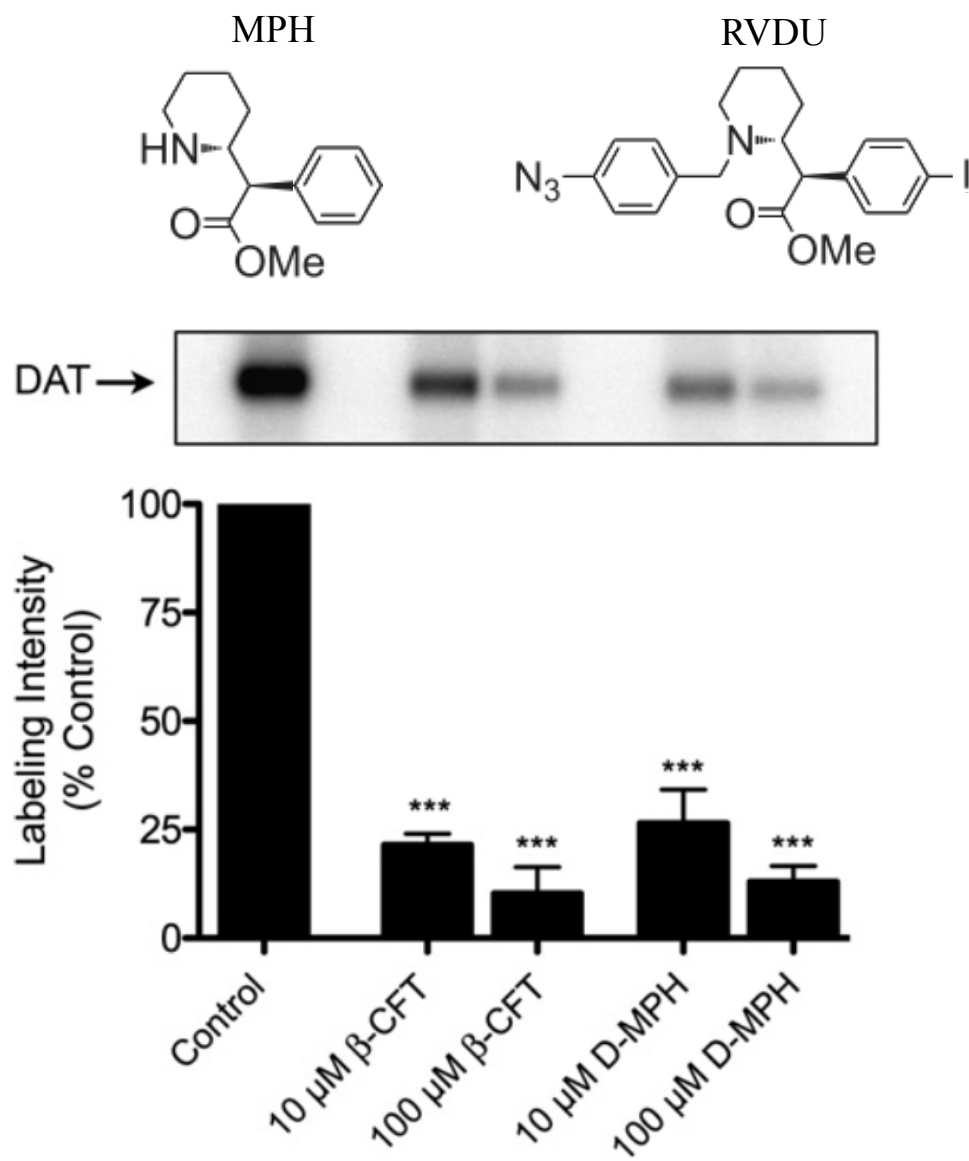
MPH

RVDU

DAT →

Photoaffinity Labeling of hDAT with Bupropion Analog ([^{125}I]SADU 3-72)

Bupropion (Wellbutrin®, Zyban®) is widely used as an antidepressant and smoking cessation agent. Because of its higher affinity towards DAT, bupropion is thought to be a likely target for treatment of cocaine dependency. However, neurochemical mechanisms of bupropion are not completely understood (103). Thus, we analyzed a novel bupropion analog ([^{125}I]SADU 3-72) for DAT photoaffinity labeling, as a first step towards understanding its interaction with DAT at the molecular level.

hDAT cells were photoaffinity labeled with [^{125}I]SADU 3-72 in the absence or presence of 10 µM or 100 µM (±)-bupropion or (-)-cocaine (Figure 22). Cells were lysed and immunoprecipitated, followed by SDS-PAGE/autoradiography. Labeling of DAT with [^{125}I]SADU 3-72 was set at 100%. Incorporation of the ligand was blocked by both (±)-bupropion or (-)-cocaine by 40-70% in a dose dependent manner. This indicates pharmacological specificity of [^{125}I]SADU 3-72 for DAT. Most importantly, this is the first successful example of DAT PAL based on a bupropion scaffold.

Figure 22: Photoaffinity labeling of DAT with [^{125}I]SADU 3-72. Structures of bupropion and SADU 3-72 are depicted on top. LLC-PK$_1$ expressing His-hDAT were photoaffinity labeled with [^{125}I]SADU 3-72 in the absence of presence of 10 μM or 100 μM (±)-bupropion or (-)-cocaine. Cells were solubilized and DATs were immunoprecipitated followed by SDS-PAGE and autoradiography. The relevant portion of a representative autoradiograph is pictured followed by a histogram that quantifies relative band intensities. Mean ± SE of three independent experiments is shown; ***p<0.0001 versus control; **p<0.001 versus control.
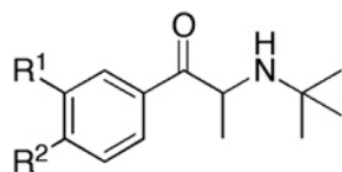
R[1] = -Cl, R[2] = -H, Bupropion

R[1] = -I, R[2] = -N$_3$, SADU-3-72

^{125}I-hDAT
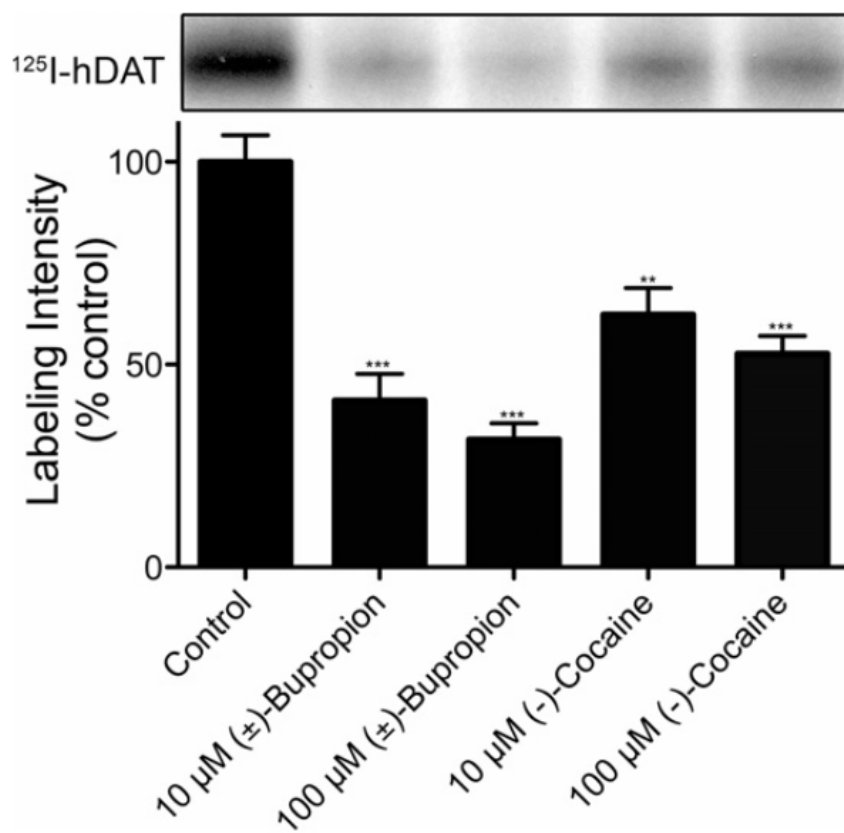
CHAPTER IV

DICUSSION

The kinetic interactions of DAT with cocaine and its analogs are complex, resulting in high and low affinity binding states (110, 111) and competitive and non-competitive uptake inhibition (112, 113). We currently lack a complete mechanistic understanding of these properties, as some mutagenesis and comparative modeling studies support the interaction of cocaine at S1 where it could suppress transport by competing with substrate for key interactions (43, 114). Furthermore, two things cannot occupy the same 3D space. On the other hand, some studies support binding near S2 where it could allosterically stabilize an inactive state of the transporter (44, 115–117). It has been proposed that these binding modes are not mutually exclusive and that cocaine may initially bind near the S2 site before transitioning to S1 following conformational changes (44, 115).

The current collection of LeuT and dDAT crystal structures supports multiple binding sites for substrates and inhibitors (37, 65, 77, 90, 107, 117–122) and both allosteric and competitive inhibition mechanisms (64, 65, 74, 77, 89, 117–120, 123–129). Understanding DAT-cocaine interaction at the molecular level is essential in order to develop any drugs to treat cocaine dependency. However, to date, no high-resolution crystal structures of cocaine-bound SLC6 transporters have been obtained (64, 123, 130)

thus, the exact cocaine binding site(s) on DAT and their relationships to the various kinetic states remain unresolved.

As a positive function approach to these issues we used irreversible cocaine analogs, [^{125}I]RTI 82, [^{125}I]MFZ 2-24, [^{125}I]JHC 2-48, as probes for physical identification of ligand interaction sites (100, 101, 131). We identified the attachment site of [^{125}I]RTI 82 to Phe320. This is the first identification of a specific photoaffinity analog contact point on DAT. Phe320 functions as a gating residue on the outer margin of the S1 binding pocket and performs a crucial role in the transition between the "outward" to "outward-occluded" states by aromatic interaction with Tyr156 (107). Figure 23 showed the best RTI 82 docked complex. The phenyl azido moiety interacts with Phe319 (numbering based upon rDAT). In addition, residues homologous to Val152 (TM3) and Ser421 (TM8), which have been implicated in high-affinity antagonist binding in SERT were found as contact points for RTI 82 binding (74, 89). Our data suggest [^{125}I]RTI 82 adduction is near the S1 site and thus, the cocaine pharmacophore most likely lies in the S1 site. This hypothesis was confirmed by cysteine protection studies as RTI 82 protected only the residues thought to line the S1 site.

We also showed that the [^{125}I]MFZ 2-24 adduction site is either D79 or L80. D79 is an essential amino acid for DA function as its negative charge coordinates the positive charge of DA and possibly of cocaine. Mutagenesis of D79 and L80 impact DA binding and its potency to inhibit CFT binding (43, 68). This data also implies that [^{125}I]MFZ 2-24 adducts close to the S1 site and thus, the cocaine pharmacophore lies in the S1 site.

[^{125}I]RTI 82 and [^{125}I]MFZ 2-24 labeling of DAT occurs with appropriate pharmacology (100, 101), and because our photolabeling analyses utilized 5 nM ligand,

Figure 23: Computational docking of RTI 82. Best rDAT/RTI 82 docked complex based on energy and constraint fulfillment. The image depicts transmembrane domains 1, 3, 6 and 8 from the LeuT-based rDAT homology model from the crystal structure of the "outward occluded" template 2A65. RTI 82 is represented by yellow sticks and side chains of select residues are represented as lines. Dashed yellow lines indicate ligand-residue interactions between (1) azido nitrogen of RTI 82 and Phe319, (2) tropane N of RTI 82 and carboxyl oxygen of Asp79 and (3) phenyl chloride of RTI 82 and side chain N of Asn157.

TM3

Y156

F319

1

TM6

L80

N157

2

D79

3

S421

TM8

TM1
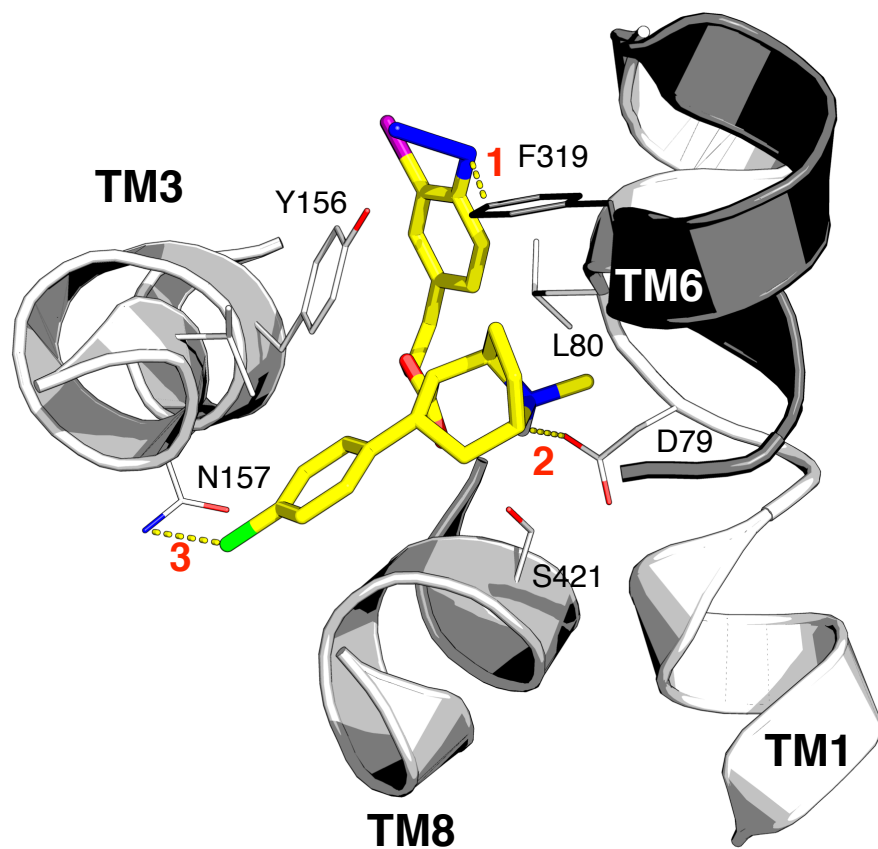
Provided by the Henry Lab, UND.

the [^{125I}]RTI 82 and [^{125I}]MFZ 2-24 attachment site identified in this study represent the high-affinity, pharmacologically relevant antagonist-bound state of the transporter. It is likely that this site closely correlates with the (–)-cocaine binding site, as the compounds share the *N*-methyl tropane pharmacophore that drives high affinity cocaine recognition (132). [^{125}I]RTI 82 differs from cocaine only in the substitution of the 3β benzoyl ester with a phenylchloride and addition of the 2β ethyl aryliodoazido moiety. [^{125}I]MFZ 2-24 differs from cocaine only in the substitution of the 3β benzoyl ester with a phenylchloride and addition of the aryliodoazido moiety from the tropane N.

We used our data in conjunction with computational docking molecular modeling studies with comparative DAT models and protection analyses to directly demonstrate binding of the tropane pharmacophore, which drives the major component of cocaine analog binding, in the S1 site (132). These findings further enhance our knowledge about cocaine-DAT molecular interactions. Based upon modeling data, the cocaine pharmacophore of [^{125}I]RTI 82 and [^{125}I]MFZ 2-24 overlap in the S1 site.

The third high affinity cocaine analog [^{125}I]JHC 2-48 analyzed also displays appropriate pharmacology as DAT inhibitors were able to displace its labeling and NET and SERT specific inhibitors failed to do so. The phenylazido moiety of this analog possibly adducts to a residue in TM 11 or 12 since Ab C-20 immunoprecipitated a ~ 12 kDa fragment. However, there is a possibility of discrepancy between electrophoretic mobility shift and the fragment size. If that were the case, then [^{125}I]JHC 2-48 adduction could occur within TMs 9-10 as well. Thus, at this point we are not able to determine the domain of [^{125}I]JHC 2-48 adduction. However, we are able to eliminate the first three TMs as the region of adduction based upon a lack of a photolabeled fragment in N-

terminal Ab pull down. The contact points provided by CNBr and trypsin peptide mapping were used to triangulate the orientation of the cocaine pharmacophore via computational modeling, which demonstrates the cocaine pharmacophores of all the analogs overlap in the S1 site supporting a competitive mechanism of cocaine (Figure 24).

The direct identification of photoaffinity ligand adduction sites confers major advantages for computational analyses of ligand poses by dramatically reducing the conformational space that must be sampled during docking analysis, and by providing experimentally-determined ligand-protein contact points can be used as absolute requirements by which recovered binding poses can be filtered. This significantly enhances the confidence with which poses can be interpreted and further analyzed by computational and mutational strategies to clarify overall transport and transport inhibition mechanisms. In addition, these procedures can be performed in functional mammalian transporters in which the WT form is directly compared to transport- and binding-competent mutant forms, which strongly increases the likelihood that physiologically relevant structures are being assessed. These multiple strengths support the utilization of this approach in further predictive docking analyses of these and other categories of DAT ligands. This is important because to date no SLC6 transporters have been co-crystalized with cocaine-like compounds or atypical DAT inhibitors, and because the uncertain structural and functional relationships between mammalian transporters and the mutation-stabilized dDAT and LeuT/SERT hybrid homologs may obscure significant differences in the transport and inhibitor binding properties of the proteins (107, 122). The tremendous sociological and economical impacts of cocaine addiction make basic understanding the mechanisms of cocaine binding and transport an

Figure 24: Computational docking of [125I]RTI 82, [125I]MFZ 2-24, and [125I]JHC 2-48.[^{125}I]RTI 82 is depicted in yellow, [^{125}I]MFZ 2-24 is depicted in black and [^{125}I]JHC 2-48 is depicted in pink. The azido moieties of these analogs are depicted in purple. The cocaine pharmacophore of these analogs overlap in the S1 pocket as represented by the blue circle.
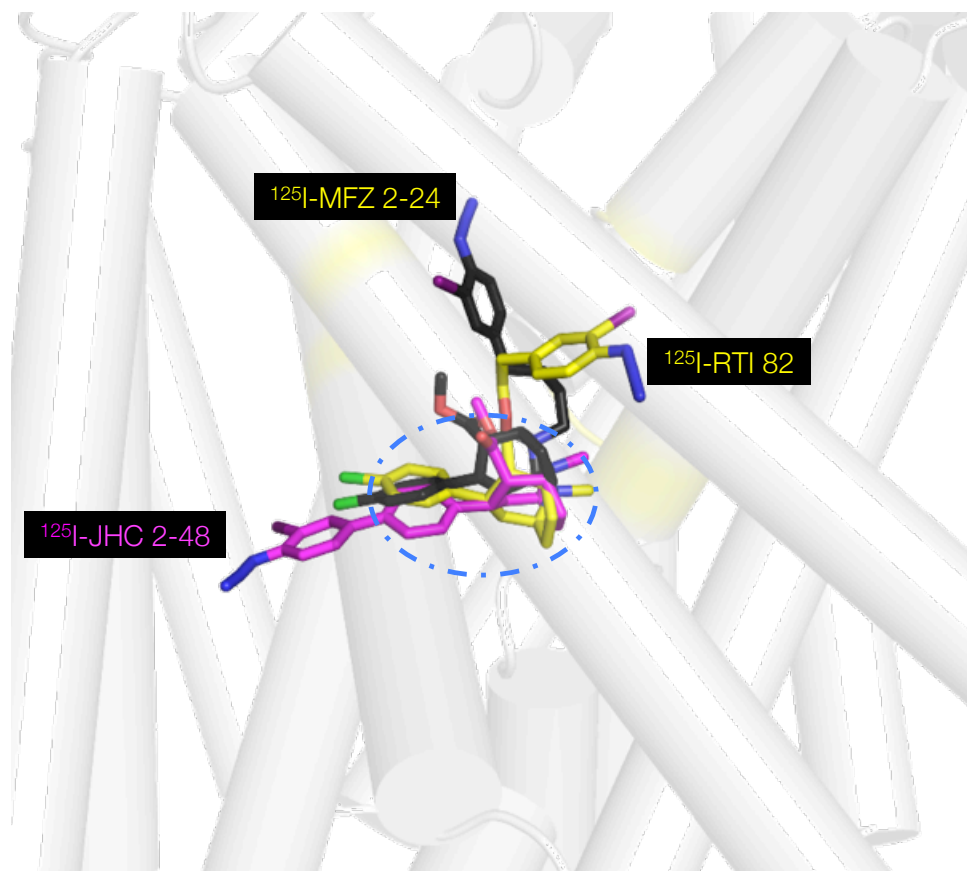
Provided by the Henry Lab, UND

important effort, especially with the promise afforded by the identification of the benztropine class of DAT antagonists, which bind to DAT and block DA uptake but do not produce the cocaine-like behavioral profiles and reduce cocaine self-administration in animal models (133, 134). It has been suggested that the benztropines may bind distinct conformations of DAT and/or possess a slow rate of occupancy following administration which may modulate the psychotropic effects of increased synaptic DA (43, 93, 133, 134).

Identification of cocaine binding residues would be valuable for rational design of novel agents that can selectively inhibit cocaine binding as antagonists, without (or with little) effect on the dopamine uptake. Cocaine binds to DAT and stabilizes the transporter in an open to out confirmation thereby preventing DA translocation. Benztropine is predicted to stabilize DAT in outward open occulted confirmation. In addition, although benztropine is predicted to bind in the S1 site and thus, overlap with the DA binding site, residues involved in benztropine binding are non-identical to residues involved in DA or CFT binding (43, 93, 114). Different conformations of DAT stabilized by various inhibitors could be further explored to understand DAT-inhibitor relation in regards to reinforcing effects.

In this study, we also analyzed novel PALs generated based upon MPH and bupropion scaffold. MPH is a typical DAT blocker while bupropion is an atypical DAT blocker. Our preliminary photoaffinity studies showed these novel PALs adduct to DAT with pharmacological specificity. This opens the possibility of utilizing these PALs for peptide mapping in order to identify their adduction sites.

Recently, modafinil and its *R*-enantiomer (Armodafinil) have also been described as having distinctive interactions at DAT that might contribute to their non-addictive and

therapeutic profiles (116, 135–137). Thus, understanding cocaine binding in relation to compounds like these atypical DAT inhibitors could provide critical insights for developing medication strategies toward treating cocaine addiction. Furthermore, the synergistic approach of photoaffinity labeling and computational modeling described here provides a benchmark that validates the use of these methods to investigate the binding sites for typical and atypical NSS inhibitors.

APPENDIX

Site-directed Mutagenesis Primers (hDAT)

The primers used for site-directed mutagenesis by the QuikChange® method are shown below.

NAME	SEQUENCE
L70M	
Sense	5'- GGGCAAGAAGATCGACTTTATGCTGTCCGTCATTGGCTT-3'
Antisense	5'-AAAGCCCAATGACGGACAGCATAAAGTCGATCTTCTTGCCC-3'
F76M	
Sense	5'-CTGTCCGTCATTGGCATGGCTGTGGACCTGGCC-3'
Antisense	5'-GGCCAGGTCCACAGCCATGCCAATGACGGACAG -3'
V73M	
Sense	5'-ATCGACTTTCTCCTGTCCATGATTGGCTTTGCTGTGGAC-3'
Antisense	5'-GTCCACAGCAAAGCCAATCATGGACAGGAGAAAGTCGAT-3'
V318M	
Sense	5'-GCGGCCACCCAGATGTGCTTCTCCC-3'
Antisense	5'-GGGAGAAGCACATCTGGGTGGCCGC-3'
I330M	
Sense	5'-GTTCGGGGTGCTGATGGCCTTCTCCAG-3'
Antisense	5'-CTGGAGAAGGCCATCAGCACCCCGAAC-3'
M272L	
Sense	5'-GGATCACAGCCACCTTGCCATACGTGGT-3'
Antisense	5'-ACCACGTATGGCAAGGTGGCTGTGATCC-3'
C319M	
Sense	5'-GCGGCCACCCAGGTGATGTTCTCCCTGGGCGTG-3'
Antisense	5'-CACGCCCAGGGAGAACATCACCTGGGTGGCCGC-3'
F320M	
Sense	5'-CACCCAGGTGTGCATGTCCCTGGGCGTGG-3'
Antisense	5'-CCACGCCCAGGGACATGCACACCTGGGTG-3'

L322M
Sense   5'-GGTGTGCTTCTCCATGGGCGTGGGGTT-3'
Antisense   5'-AACCCCACGCCCATGGAGAAGCACACC-3'

V324M
Sense   5'-TTCTCCCTGGGCATGGGGTTCGGGG-3'
Antisense   5'-CCCCGAACCCCATGCCCAGGGAGAA-3'

G325M
Sense   5'-CTCCCTGGGCGTGATGTTCGGGGTGCTG-3'
Antisense   5'-CAGCACCCCGAACATCACGCCCAGGGAG-3'

F326M
Sense   5'-CCTGGGCGTGGGGATGGGGGTGCTGATCG-3'
Antisense   5'-CGATCAGCACCCCCATCCCCACGCCCAGG-3'

V328M
Sense   5'-CGTGGGGTTCGGGATGCTGATCGCCTT-3'
Antisense   5'-AAGGCGATCAGCATCCCGAACCCCACG-3'

L329M
Sense   5'-GGGGTTCGGGGTGATGATCGCCTTCTC-3'
Antisense   5'-GAGAAGGCGATCATCACCCCGAACCCC-3'

D79M
Sense   5'-TCATTGGCTTTGCTGTGATGCTGGCCAACGTCTGGCG-3'
Antisense   5'-CGCCAGACGTTGGCCAGCATCACAGCAAAGCCAATGA-3'

S321M
Sense   5'-ACCCAGGTGTGCTTCATGCTGGGCGTGGGGTTC-3'
Antisense   5'-GAACCCCACGCCCAGCATGAAGCACACCTGGGT-3'

M371L
Sense   5'-GTGCTTCTGTGCCAAGTACCCCAGGAAGG-3'
Antisense   5'-CCTTCCTGGGGTACTTGGCACAGAAGCAC-3'

The primers used for site-directed mutagenesis by the QuikChange® method are shown below.

NAME	SEQUENCE

F76M
Sense   5'-CTATCAGTCATCGGCATGGCTGTGGACCTGGCC-3'
Antisense   5'-GGCCAGGTCCACAGCCATGCCGATGACTGATAG-3'

V73M
Sense   5'-CAAGAAAATTGATTTCCTGCTATCAATGATCGGCTTTGCTGTGGA-3'
Antisense   5'-TCCACAGCAAAGCCGATCATTGATAGCAGGAAATCAATTTTCTTG-3'

L70M
Sense   5'-GGAGCAAGAAAATTGATTTCATGCTATCAGTCATCGGC-3'
Antisense   5'-GCCGATGACTGATAGCATGAAATCAATTTTCTTGCTCC-3'

I74M
Sense   5'-ATTTCCTGCTATCAGTCATGGGCTTTGCTGTGGA-3'
Antisense   5'-TCCACAGCAAAGCCCATGACTGATAGCAGGAAAT-3'

G75M
Sense   5'-GATTTCCTGCTATCAGTCATCATGTTTGCTGTGGACCTGGCCAAT-3'
Antisense   5'-ATTGGCCAGGTCCACAGCAAACATGATGACTGATAGCAGGAAATC-3'

A77M
Sense   5'-CTGCTATCAGTCATCGGCTTTATGGTGGACCTGGCCAATGTCT-3'
Antisense   5'-AGACATTGGCCAGGTCCACCATAAAGCCGATGACTGATAGCAG-3'

V78M
Sense   5'-CTATCAGTCATCGGCTTTGCTATGGACCTGGCC-3'
Antisense   5'-GGCCAGGTCCATAGCAAAGCCGATGACTGATAG-3'

L80M
Sense   5'-GGCTTTGCTGTGGACATGGCCAATGTCTGGA-3'
Antisense   5'-TCCAGACATTGGCCATGTCCACAGCAAAGCC-3'

M570L
Sense   5'-CACATCCTCCATGGCCTTGGTGCCCATTTATGC-3'
Antisense   5'-GCATAAATGGGCACCAAGGCCATGGAGGATGTG-3'

M568L
Sense   5'-CGCCACATCCTCCTTGGCCATGGTGCC-3'
Antisense   5'-GGCACCATGGCCAAGGAGGATGTGGCG-3'
M568L/

M570L
Sense   5'-CGCCACATCCTCCTTGGCCTTGGTGCCCATTTA-3'
Antisense   5'-TAAATGGGCACCAAGGCCAAGGAGGATGTGGCG-3'

A569M
Sense   5'-CATCGCCACATCCTCCATGATGATGGTGCCCATTTATGCGA-3'
Antisense   5'-TCGCATAAATGGGCACCATCATCATGGAGGATGTGGCGATG-3'

M11L
Sense   5'-ATGCTCCGTGGGACCATTGTCTTCAGTGGTG-3'
Antisense   5'-CACCACTGAAGACAATGGTCCCACGGAGCAT-3'

M510L
Sense   5'-TTCAGTGATGACATCAAGCAATTGACAGGGCAGC-3'
Antisense   5'-GCTGCCCTGTCAATTGCTTGATGTCATCACTGAA-3'

REFERENCES

1. Carlsson, A. (1959) The occurrence, distribution and physiological role of catecholamines in the nervous system. *Pharmacol. Rev.* **11**, 490–3 [online] http://www.ncbi.nlm.nih.gov/pubmed/13667431

2. Carlsson, A. (1993) Thirty years of dopamine research. *Adv. Neurol.* **60**, 1–10 [online] http://www.ncbi.nlm.nih.gov/pubmed/8093570

3. Yeragani, V. K., Tancer, M., Chokka, P., and Baker, G. B. (2010) Arvid Carlsson, and the story of dopamine. *Indian J. Psychiatry* **52**, 87–8 [online] http://www.pubmedcentral.nih.gov/articlerender.fcgi?artid=2824994&tool=pmcentrez&rendertype=abstract

4. Elsworth, J. D., and Roth, R. H. (1997) Dopamine synthesis, uptake, metabolism, and receptors: relevance to gene therapy of Parkinson's disease. *Exp. Neurol.* **144**, 4–9 [online] http://www.sciencedirect.com/science/article/pii/S0014488696963797

5. Vergo, S., Johansen, J. L., Leist, M., and Lotharius, J. (2007) Vesicular monoamine transporter 2 regulates the sensitivity of rat dopaminergic neurons to disturbed cytosolic dopamine levels. *Brain Res.* **1185**, 18–32 [online] http://www.sciencedirect.com/science/article/pii/S0006899307022147

6. Grace, A. A., and Bunney, B. S. (1984) The control of firing pattern in nigral dopamine neurons: burst firing. *J. Neurosci.* **4**, 2877–90 [online] http://www.ncbi.nlm.nih.gov/pubmed/6150071

7. Falck, B., Hillarp, N. A., Thieme, G., and Torp, A. (1982) Fluorescence of catechol amines and related compounds condensed with formaldehyde. *Brain Res. Bull.* **9**, xi–xv [online] http://www.ncbi.nlm.nih.gov/pubmed/7172023

8. Grace, A. A., and Bunney, B. S. (1980) Nigral dopamine neurons: intracellular recording and identification with L-dopa injection and histofluorescence. *Science* **210**, 654–6 [online] http://www.ncbi.nlm.nih.gov/pubmed/7433992

9. Bunney, B. S., Walters, J. R., Roth, R. H., and Aghajanian, G. K. (1973) Dopaminergic neurons: effect of antipsychotic drugs and amphetamine on single cell activity. *J. Pharmacol. Exp. Ther.* **185**, 560–71 [online] http://www.ncbi.nlm.nih.gov/pubmed/4576427

10. Grace, A. A., and Bunney, B. S. (1983) Intracellular and extracellular electrophysiology of nigral dopaminergic neurons--1. Identification and characterization. *Neuroscience* **10**, 301–15 [online] http://www.ncbi.nlm.nih.gov/pubmed/6633863

11. Björklund, A., and Dunnett, S. B. (2007) Dopamine neuron systems in the brain: an update. *Trends Neurosci.* **30**, 194–202 [online] http://www.ncbi.nlm.nih.gov/pubmed/17408759

12. Guastella, J., Nelson, N., Nelson, H., Czyzyk, L., Keynan, S., Miedel, M. C., Davidson, N., Lester, H. A., and Kanner, B. I. (1990) Cloning and expression of a rat brain GABA transporter. *Science* **249**, 1303–6 [online] http://www.ncbi.nlm.nih.gov/pubmed/1975955

13. Chen, J. G., Liu-Chen, S., and Rudnick, G. (1998) Determination of external loop topology in the serotonin transporter by site-directed chemical labeling. *J. Biol. Chem.* **273**, 12675–81 [online] http://www.ncbi.nlm.nih.gov/pubmed/9575231

14. Pacholczyk, T., Blakely, R. D., and Amara, S. G. (1991) Expression cloning of a cocaine- and antidepressant-sensitive human noradrenaline transporter. *Nature* **350**, 350–4 [online] http://www.ncbi.nlm.nih.gov/pubmed/2008212

15. Giros, B., el Mestikawy, S., Godinot, N., Zheng, K., Han, H., Yang-Feng, T., and Caron, M. G. (1992) Cloning, pharmacological characterization, and chromosome assignment of the human dopamine transporter. *Mol. Pharmacol.* **42**, 383–90 [online] http://www.ncbi.nlm.nih.gov/pubmed/1406597

16. Stockner, T., Montgomery, T. R., Kudlacek, O., Weissensteiner, R., Ecker, G. F., Freissmuth, M., and Sitte, H. H. (2013) Mutational analysis of the high-affinity zinc binding site validates a refined human dopamine transporter homology model. *PLoS Comput. Biol.* **9**, e1002909 [online] http://dx.plos.org/10.1371/journal.pcbi.1002909

17. Norgaard-Nielsen, K., Norregaard, L., Hastrup, H., Javitch, J. a, and Gether, U. (2002) Zn(2+) site engineering at the oligomeric interface of the dopamine transporter. *FEBS Lett.* **524**, 87–91 [online] http://www.ncbi.nlm.nih.gov/pubmed/12135746.

18. Vaughan, R. A., Huff, R. A., Uhl, G. R., and Kuhar, M. J. (1997) Protein Kinase C-mediated Phosphorylation and Functional Regulation of Dopamine Transporters in Striatal Synaptosomes. *J. Biol. Chem.* **272**, 15541–15546 [online] http://www.jbc.org/content/272/24/15541.abstract?ijkey=7376fcfa6df928abd4756757f7e58da7f43f600e&keytype2=tf_ipsecsha

19. Moritz, A. E., Foster, J. D., Gorentla, B. K., Mazei-Robison, M. S., Yang, J.-W., Sitte, H. H., Blakely, R. D., and Vaughan, R. A. (2013) Phosphorylation of dopamine transporter serine 7 modulates cocaine analog binding. *J. Biol. Chem.* **288**, 20–32 [online] http://www.pubmedcentral.nih.gov/articlerender.fcgi?artid=3537014&tool=pmcentrez&rendertype=abstract

20. Steinkellner, T., Yang, J.-W., Montgomery, T. R., Chen, W.-Q., Winkler, M.-T., Sucic, S., Lubec, G., Freissmuth, M., Elgersma, Y., Sitte, H. H., and Kudlacek, O. (2012) Ca(2+)/calmodulin-dependent protein kinase IIα (αCaMKII) controls the activity of the dopamine transporter: implications for Angelman syndrome. *J. Biol. Chem.* **287**, 29627–

35 [online]
http://www.pubmedcentral.nih.gov/articlerender.fcgi?artid=3436163&tool=pmcentrez&re
ndertype=abstract

21.   Foster, J. D., Cervinski, M. A., Gorentla, B. K., and Vaughan, R. A. (2006) Regulation of
       the dopamine transporter by phosphorylation. *Handb. Exp. Pharmacol.*, 197–214 [online]
       http://www.ncbi.nlm.nih.gov/pubmed/16722237

22.   Foster, J. D., Yang, J.-W., Moritz, A. E., Challasivakanaka, S., Smith, M. A., Holy, M.,
       Wilebski, K., Sitte, H. H., and Vaughan, R. A. (2012) Dopamine transporter
       phosphorylation site threonine 53 regulates substrate reuptake and amphetamine-
       stimulated efflux. *J. Biol. Chem.* **287**, 29702–12 [online]
       http://www.pubmedcentral.nih.gov/articlerender.fcgi?artid=3436161&tool=pmcentrez&re
       ndertype=abstract

23.   Linder, M. E., and Deschenes, R. J. (2007) Palmitoylation: policing protein stability and
       traffic. *Nat. Rev. Mol. Cell Biol.* **8**, 74–84 [online]
       http://www.ncbi.nlm.nih.gov/pubmed/17183362

24.   Draper, J. M., Xia, Z., and Smith, C. D. (2007) Cellular palmitoylation and trafficking of
       lipidated peptides. *J. Lipid Res.* **48**, 1873–84 [online]
       http://www.pubmedcentral.nih.gov/articlerender.fcgi?artid=2895159&tool=pmcentrez&re
       ndertype=abstract

25.   Greaves, J., and Chamberlain, L. H. (2007) Palmitoylation-dependent protein sorting. *J.
       Cell Biol.* **176**, 249–54 [online]
       http://www.pubmedcentral.nih.gov/articlerender.fcgi?artid=2063950&tool=pmcentrez&re
       ndertype=abstract

26.   Foster, J. D., and Vaughan, R. A. (2011) Palmitoylation controls dopamine transporter
       kinetics, degradation, and protein kinase C-dependent regulation. *J. Biol. Chem.* **286**,
       5175–86 [online] http://www.jbc.org/content/286/7/5175.full

27.   Miranda, M., Dionne, K. R., Sorkina, T., and Sorkin, A. (2007) Three ubiquitin
       conjugation sites in the amino terminus of the dopamine transporter mediate protein
       kinase C-dependent endocytosis of the transporter. *Mol. Biol. Cell* **18**, 313–23 [online]
       http://www.pubmedcentral.nih.gov/articlerender.fcgi?artid=1751334&tool=pmcentrez&re
       ndertype=abstract

28.   Miranda, M., Wu, C. C., Sorkina, T., Korstjens, D. R., and Sorkin, A. (2005) Enhanced
       ubiquitylation and accelerated degradation of the dopamine transporter mediated by
       protein kinase C. *J. Biol. Chem.* **280**, 35617–24 [online]
       http://www.ncbi.nlm.nih.gov/pubmed/16109712

29.   Kuhar, M. J. (1996) Dopamine Transporter Ligand Binding Domains. STRUCTURAL AND FUNCTIONAL PROPERTIES REVEALED BY LIMITED PROTEOLYSIS. *J. Biol. Chem.* **271**, 21672–21680 [online] http://www.jbc.org/content/271/35/21672.long

30.   Torres, G. E., Carneiro, A., Seamans, K., Fiorentini, C., Sweeney, A., Yao, W.-D., and Caron, M. G. (2003) Oligomerization and trafficking of the human dopamine transporter. Mutational analysis identifies critical domains important for the functional expression of the transporter. *J. Biol. Chem.* **278**, 2731–9 [online] http://www.ncbi.nlm.nih.gov/pubmed/12429746

31.   Li, L.-B., Chen, N., Ramamoorthy, S., Chi, L., Cui, X.-N., Wang, L. C., and Reith, M. E. A. (2004) The role of N-glycosylation in function and surface trafficking of the human dopamine transporter. *J. Biol. Chem.* **279**, 21012–20 [online] http://www.ncbi.nlm.nih.gov/pubmed/15024013

32.   Chen, R., Wei, H., Hill, E. R., Chen, L., Jiang, L., Han, D. D., and Gu, H. H. (2007) Direct evidence that two cysteines in the dopamine transporter form a disulfide bond. *Mol. Cell. Biochem.* **298**, 41–8 [online] http://www.ncbi.nlm.nih.gov/pubmed/17131045

33.   Wang, J. B., Moriwaki, A., and Uhl, G. R. (1995) Dopamine transporter cysteine mutants: second extracellular loop cysteines are required for transporter expression. *J. Neurochem.* **64**, 1416–9 [online] http://www.ncbi.nlm.nih.gov/pubmed/7861176

34.   Fog, J. U., Khoshbouei, H., Holy, M., Owens, W. A., Vaegter, C. B., Sen, N., Nikandrova, Y., Bowton, E., McMahon, D. G., Colbran, R. J., Daws, L. C., Sitte, H. H., Javitch, J. A., Galli, A., and Gether, U. (2006) Calmodulin kinase II interacts with the dopamine transporter C terminus to regulate amphetamine-induced reverse transport. *Neuron* **51**, 417–29 [online] http://www.ncbi.nlm.nih.gov/pubmed/16908408

35.   Cervinski, M. A., Foster, J. D., and Vaughan, R. A. (2010) Syntaxin 1A regulates dopamine transporter activity, phosphorylation and surface expression. *Neuroscience* **170**, 408–16 [online] http://www.pubmedcentral.nih.gov/articlerender.fcgi?artid=2933327&tool=pmcentrez&rendertype=abstract

36.   Torres, G. E. (2006) The dopamine transporter proteome. *J. Neurochem.* **97 Suppl 1**, 3–10 [online] http://www.ncbi.nlm.nih.gov/pubmed/16635244

37.   Yamashita, A., Singh, S. K., Kawate, T., Jin, Y., and Gouaux, E. (2005) Crystal structure of a bacterial homologue of Na+/Cl--dependent neurotransmitter transporters. *Nature* **437**, 215–23 [online] http://www.ncbi.nlm.nih.gov/pubmed/16041361

38.   Beuming, T., Shi, L., Javitch, J., and Weinstein, H. (2006) A comprehensive structure-based alignment of prokaryotic and eukaryotic neurotransmitter/Na+ symporters (NSS) aids in the use of the LeuT structure to probe NSS structure and function. *Mol. Pharmacol.* **70**, 1630–42

39. Zomot, E., Bendahan, A., Quick, M., Zhao, Y., Javitch, J. A., and Kanner, B. I. (2007) Mechanism of chloride interaction with neurotransmitter:sodium symporters. *Nature* **449**, 726–30 [online] http://www.ncbi.nlm.nih.gov/pubmed/17704762 (Accessed February 20, 2014).

40. Kantcheva, A. K., Quick, M., Shi, L., Winther, A.-M. L., Stolzenberg, S., Weinstein, H., Javitch, J. A., and Nissen, P. (2013) Chloride binding site of neurotransmitter sodium symporters. *Proc. Natl. Acad. Sci. U. S. A.* **110**, 8489–94 [online] http://www.pubmedcentral.nih.gov/articlerender.fcgi?artid=3666746&tool=pmcentrez&re ndertype=abstract

41. Forrest, L. R., Tavoulari, S., Zhang, Y.-W., Rudnick, G., and Honig, B. (2007) Identification of a chloride ion binding site in Na+/Cl -dependent transporters. *Proc. Natl. Acad. Sci. U. S. A.* **104**, 12761–6 [online] http://www.pubmedcentral.nih.gov/articlerender.fcgi?artid=1937540&tool=pmcentrez&re ndertype=abstract

42. Tavoulari, S., Rizwan, A. N., Forrest, L. R., and Rudnick, G. (2011) Reconstructing a chloride-binding site in a bacterial neurotransmitter transporter homologue. *J. Biol. Chem.* **286**, 2834–42 [online] http://www.pubmedcentral.nih.gov/articlerender.fcgi?artid=3024779&tool=pmcentrez&re ndertype=abstract

43. Beuming, T., Kniazeff, J., and Bergmann, M. (2008) The binding sites for cocaine and dopamine in the dopamine transporter overlap. *Nat. ...* **11**, 780–9 [online] http://www.pubmedcentral.nih.gov/articlerender.fcgi?artid=2692229&tool=pmcentrez&re ndertype=abstract

44. Huang, X., Gu, H. H., and Zhan, C.-G. (2009) Mechanism for cocaine blocking the transport of dopamine: insights from molecular modeling and dynamics simulations. *J. Phys. Chem. B* **113**, 15057–66 [online] http://www.pubmedcentral.nih.gov/articlerender.fcgi?artid=2774931&tool=pmcentrez&re ndertype=abstract

45. Ritz, M. C., Lamb, R. J., Goldberg, S. R., and Kuhar, M. J. (1987) Cocaine receptors on dopamine transporters are related to self-administration of cocaine. *Science* **237**, 1219–23 [online] http://www.ncbi.nlm.nih.gov/pubmed/2820058.

46. Seiden, L. S., Sabol, K. E., and Ricaurte, G. A. (1993) Amphetamine: effects on catecholamine systems and behavior. *Annu. Rev. Pharmacol. Toxicol.* **33**, 639–77 [online] http://www.ncbi.nlm.nih.gov/pubmed/8494354

47. Kahlig, K. M., Binda, F., Khoshbouei, H., Blakely, R. D., McMahon, D. G., Javitch, J. A., and Galli, A. (2005) Amphetamine induces dopamine efflux through a dopamine transporter channel. *Proc. Natl. Acad. Sci. U. S. A.* **102**, 3495–500 [online]

http://www.pubmedcentral.nih.gov/articlerender.fcgi?artid=549289&tool=pmcentrez&ren
dertype=abstract

48.   Kuhar, M. J., Ritz, M. C., and Boja, J. W. (1991) The dopamine hypothesis of the
      reinforcing properties of cocaine. *Trends Neurosci.* **14**, 299–302 [online]
      http://www.ncbi.nlm.nih.gov/pubmed/1719677

49.   Giros, B., Jaber, M., Jones, S. R., Wightman, R. M., and Caron, M. G. (1996)
      Hyperlocomotion and indifference to cocaine and amphetamine in mice lacking the
      dopamine transporter. *Nature* **379**, 606–12 [online]
      http://www.ncbi.nlm.nih.gov/pubmed/8628395

50.   Rocha, B. a, Fumagalli, F., Gainetdinov, R. R., Jones, S. R., Ator, R., Giros, B., Miller, G.
      W., and Caron, M. G. (1998) Cocaine self-administration in dopamine-transporter
      knockout mice. *Nat. Neurosci.* **1**, 132–7 [online]
      http://www.ncbi.nlm.nih.gov/pubmed/10195128.

51.   Sora, I., Wichems, C., Takahashi, N., Li, X. F., Zeng, Z., Revay, R., Lesch, K. P., Murphy,
      D. L., and Uhl, G. R. (1998) Cocaine reward models: conditioned place preference can be
      established in dopamine- and in serotonin-transporter knockout mice. *Proc. Natl. Acad.
      Sci. U. S. A.* **95**, 7699–704 [online]
      http://www.pubmedcentral.nih.gov/articlerender.fcgi?artid=22727&tool=pmcentrez&rend
      ertype=abstract

52.   Hall, F. S., Li, X. F., Sora, I., Xu, F., Caron, M., Lesch, K. P., Murphy, D. L., and Uhl, G.
      R. (2002) Cocaine mechanisms: enhanced cocaine, fluoxetine and nisoxetine place
      preferences following monoamine transporter deletions. *Neuroscience* **115**, 153–61
      [online] http://www.ncbi.nlm.nih.gov/pubmed/12401330

53.   Hall, F. S., Sora, I., Drgonova, J., Li, X.-F., Goeb, M., and Uhl, G. R. (2004) Molecular
      mechanisms underlying the rewarding effects of cocaine. *Ann. N. Y. Acad. Sci.* **1025**, 47–
      56 [online] http://www.ncbi.nlm.nih.gov/pubmed/15542699

54.   Thomsen, M., Hall, F. S., Uhl, G. R., and Caine, S. B. (2009) Dramatically decreased
      cocaine self-administration in dopamine but not serotonin transporter knock-out mice. *J.
      Neurosci.* **29**, 1087–92 [online]
      http://www.pubmedcentral.nih.gov/articlerender.fcgi?artid=2745929&tool=pmcentrez&re
      ndertype=abstract

55.   Chen, R., Han, D. D., and Gu, H. H. (2005) A triple mutation in the second
      transmembrane domain of mouse dopamine transporter markedly decreases sensitivity to
      cocaine and methylphenidate. *J. Neurochem.* **94**, 352–9 [online]
      http://www.ncbi.nlm.nih.gov/pubmed/15998286

56.   Thomsen, M., Han, D. D., Gu, H. H., and Caine, S. B. (2009) Lack of cocaine self-
      administration in mice expressing a cocaine-insensitive dopamine transporter. *J.*

Pharmacol. Exp. Ther. **331**, 204–11 [online] http://www.pubmedcentral.nih.gov/articlerender.fcgi?artid=2766230&tool=pmcentrez&rendertype=abstract

57.   Chen, R., Tilley, M. R., Wei, H., Zhou, F., Zhou, F.-M., Ching, S., Quan, N., Stephens, R. L., Hill, E. R., Nottoli, T., Han, D. D., and Gu, H. H. (2006) Abolished cocaine reward in mice with a cocaine-insensitive dopamine transporter. *Proc. Natl. Acad. Sci. U. S. A.* **103**, 9333–8 [online] http://www.pubmedcentral.nih.gov/articlerender.fcgi?artid=1482610&tool=pmcentrez&rendertype=abstract

58.   Volkow, N. D. (2000) Addiction, a Disease of Compulsion and Drive: Involvement of the Orbitofrontal Cortex. *Cereb. Cortex* **10**, 318–325 [online] http://cercor.oxfordjournals.org/content/10/3/318.full

59.   Volkow, N. D., Wang, G. J., Fischman, M. W., Foltin, R. W., Fowler, J. S., Abumrad, N. N., Vitkun, S., Logan, J., Gatley, S. J., Pappas, N., Hitzemann, R., and Shea, C. E. (1997) Relationship between subjective effects of cocaine and dopamine transporter occupancy. *Nature* **386**, 827–30 [online] http://www.ncbi.nlm.nih.gov/pubmed/9126740

60.   WIilbrandt, W., and Rosenberg, T. (1961) The concept of carrier transport and its corollaries in pharmacology. *Pharmacol. Rev.* **13**, 109–83 [online] http://www.ncbi.nlm.nih.gov/pubmed/13785205

61.   Mitchell, P. (1957) A General Theory of Membrane Transport From Studies of Bacteria. *Nature* **180**, 134–136 [online] http://www.nature.com/doifinder/10.1038/180134a0

62.   Jardetzky, O. (1966) Simple allosteric model for membrane pumps. *Nature* **211**, 969–70 [online] http://www.ncbi.nlm.nih.gov/pubmed/5968307

63.   Forrest, L. R., Zhang, Y.-W., Jacobs, M. T., Gesmonde, J., Xie, L., Honig, B. H., and Rudnick, G. (2008) Mechanism for alternating access in neurotransmitter transporters. *Proc. Natl. Acad. Sci. U. S. A.* **105**, 10338–43 [online] http://www.pubmedcentral.nih.gov/articlerender.fcgi?artid=2480614&tool=pmcentrez&rendertype=abstract

64.   Kristensen, A. S., Andersen, J., Jørgensen, T. N., Sørensen, L., Eriksen, J., Loland, C. J., and Strømgaard, K. (2011) SLC6 Neurotransmitter Transporters : Structure , Function , and Regulation. **63**, 585–640

65.   Singh, S. K., Piscitelli, C. L., Yamashita, A., and Gouaux, E. (2008) A competitive inhibitor traps LeuT in an open-to-out conformation. *Science* **322**, 1655–61 [online] http://www.pubmedcentral.nih.gov/articlerender.fcgi?artid=2832577&tool=pmcentrez&rendertype=abstract

66. Krishnamurthy, H., Piscitelli, C. L., and Gouaux, E. (2009) Unlocking the molecular secrets of sodium-coupled transporters. *Nature* **459**, 347–55 [online] http://www.ncbi.nlm.nih.gov/pubmed/19458710

67. Carvelli, L., McDonald, P. W., Blakely, R. D., and Defelice, L. J. (2004) Dopamine transporters depolarize neurons by a channel mechanism. *Proc. Natl. Acad. Sci. U. S. A.* **101**, 16046–51 [online] http://www.pubmedcentral.nih.gov/articlerender.fcgi?artid=528740&tool=pmcentrez&rendertype=abstract

68. Kitayama, S., Shimada, S., Xu, H., Markham, L., Donovan, D. M., and Uhl, G. R. (1992) Dopamine transporter site-directed mutations differentially alter substrate transport and cocaine binding. *Proc. Natl. Acad. Sci. U. S. A.* **89**, 7782–5 [online] http://www.pubmedcentral.nih.gov/articlerender.fcgi?artid=49795&tool=pmcentrez&rendertype=abstract

69. Lin, Z., Wang, W., Kopajtic, T., Revay, R. S., and Uhl, G. R. (1999) Dopamine transporter: transmembrane phenylalanine mutations can selectively influence dopamine uptake and cocaine analog recognition. *Mol. Pharmacol.* **56**, 434–47 [online] http://www.ncbi.nlm.nih.gov/pubmed/10419565.

70. Chen, N., Vaughan, R. A., and Reith, M. E. A. (2001) The role of conserved tryptophan and acidic residues in the human dopamine transporter as characterized by site-directed mutagenesis. *J. Neurochem.* **77**, 1116–1127 [online] http://doi.wiley.com/10.1046/j.1471-4159.2001.00312.x

71. Uhl, G. R., and Lin, Z. (2003) The top 20 dopamine transporter mutants: structure–function relationships and cocaine actions. *Eur. J. Pharmacol.* **479**, 71–82 [online] http://linkinghub.elsevier.com/retrieve/pii/S0014299903023112

72. Lin, Z., Wang, W., and Uhl, G. R. (2000) Dopamine transporter tryptophan mutants highlight candidate dopamine- and cocaine-selective domains. *Mol. Pharmacol.* **58**, 1581–92 [online] http://www.ncbi.nlm.nih.gov/pubmed/11093799

73. Lin, Z., and Uhl, G. R. (2002) Dopamine transporter mutants with cocaine resistance and normal dopamine uptake provide targets for cocaine antagonism. *Mol. Pharmacol.* **61**, 885–91 [online] http://www.ncbi.nlm.nih.gov/pubmed/11901228

74. Henry, L. K., Field, J. R., Adkins, E. M., Parnas, M. L., Vaughan, R. a, Zou, M.-F., Newman, A. H., and Blakely, R. D. (2006) Tyr-95 and Ile-172 in transmembrane segments 1 and 3 of human serotonin transporters interact to establish high affinity recognition of antidepressants. *J. Biol. Chem.* **281**, 2012–23 [online] http://www.ncbi.nlm.nih.gov/pubmed/16272152

75. Lee, S. H., Chang, M. Y., Lee, K. H., Park, B. S., Lee, Y. S., and Chin, H. R. (2000) Importance of valine at position 152 for the substrate transport and 2beta-carbomethoxy-

3beta-(4-fluorophenyl)tropane binding of dopamine transporter. *Mol. Pharmacol.* **57**, 883–9 [online] http://www.ncbi.nlm.nih.gov/pubmed/10779370

76.   Itokawa, M., Lin, Z., Cai, N. S., Wu, C., Kitayama, S., Wang, J. B., and Uhl, G. R. (2000) Dopamine transporter transmembrane domain polar mutants: DeltaG and DeltaDeltaG values implicate regions important for transporter functions. *Mol. Pharmacol.* **57**, 1093–1103

77.   Quick, M., Winther, A.-M. L., Shi, L., Nissen, P., Weinstein, H., and Javitch, J. A. (2009) Binding of an octylglucoside detergent molecule in the second substrate (S2) site of LeuT establishes an inhibitor-bound conformation. *Proc. Natl. Acad. Sci. U. S. A.* **106**, 5563–8 [online] http://www.pnas.org/content/106/14/5563.long

78.   Shan, J., Javitch, J. A., Shi, L., and Weinstein, H. (2011) The substrate-driven transition to an inward-facing conformation in the functional mechanism of the dopamine transporter. *PLoS One* **6**, e16350 [online] http://dx.plos.org/10.1371/journal.pone.0016350

79.   Henry, L. K., Adkins, E. M., Han, Q., and Blakely, R. D. (2003) Serotonin and cocaine-sensitive inactivation of human serotonin transporters by methanethiosulfonates targeted to transmembrane domain I. *J. Biol. Chem.* **278**, 37052–63

80.   Ferrer, J. V, and Javitch, J. a (1998) Cocaine alters the accessibility of endogenous cysteines in putative extracellular and intracellular loops of the human dopamine transporter. *Proc. Natl. Acad. Sci. U. S. A.* **95**, 9238–43 [online] http://www.pubmedcentral.nih.gov/articlerender.fcgi?artid=21322&tool=pmcentrez&rendertype=abstract.

81.   Sen, N., Shi, L., Beuming, T., Weinstein, H., and Javitch, J. A. (2005) A pincer-like configuration of TM2 in the human dopamine transporter is responsible for indirect effects on cocaine binding. *Neuropharmacology* **49**, 780–790

82.   Chen, J. G., Sachpatzidis, A., and Rudnick, G. (1997) The third transmembrane domain of the serotonin transporter contains residues associated with substrate and cocaine binding. *J. Biol. Chem.* **272**, 28321–28327

83.   Carroll, F. I., Gao, Y. G., Rahman, M. A., Abraham, P., Parham, K., Lewin, A. H., Boja, J. W., and Kuhar, M. J. (1991) Synthesis, ligand binding, QSAR, and CoMFA study of 3 beta-(p-substituted phenyl)tropane-2 beta-carboxylic acid methyl esters. *J. Med. Chem.* **34**, 2719–2725

84.   Carroll, F. I., Mascarella, S. W., Kuzemko, M. A., Gao, Y., Abraham, P., Lewin, A. H., Boja, J. W., and Kuhar, M. J. (1994) Synthesis, ligand binding, and QSAR (CoMFA and classical) study of 3 beta-(3'-substituted phenyl)-, 3 beta-(4'-substituted phenyl)-, and 3 beta-(3',4'-disubstituted phenyl)tropane-2 beta-carboxylic acid methyl esters. *J. Med. Chem.* **37**, 2865–2873

85.   Wu, X., and Gu, H. H. (2003) Cocaine affinity decreased by mutations of aromatic residue phenylalanine 105 in the transmembrane domain 2 of dopamine transporter. *Mol. Pharmacol.* **63**, 653–658

86.   Meltzer, P. C., Blundell, P., Yong, Y. F., Chen, Z., George, C., Gonzalez, M. D., and Madras, B. K. (2000) 2-Carbomethoxy-3-aryl-8-bicyclo[3.2.1]octanes: Potent Non-Nitrogen Inhibitors of Monoamine Transporters. *J. Med. Chem.* **43**, 2982–2991 [online] http://dx.doi.org/10.1021/jm000191g

87.   Madras, B. K., Pristupa, Z. B., Niznik, H. B., Liang, A. Y., Blundell, P., Gonzalez, M. D., and Meltzer, P. C. (1996) Nitrogen-based drugs are not essential for blockade of monoamine transporters. *Synapse* **24**, 340–348

88.   Ukairo, O. T., Bondi, C. D., Newman, A. H., Kulkarni, S. S., Kozikowski, A. P., Pan, S., and Surratt, C. K. (2005) Recognition of benztropine by the dopamine transporter (DAT) differs from that of the classical dopamine uptake inhibitors cocaine, methylphenidate, and mazindol as a function of a DAT transmembrane 1 aspartic acid residue. *J. Pharmacol. Exp. Ther.* **314**, 575–83 [online] http://www.ncbi.nlm.nih.gov/pubmed/15879005

89.   Andersen, J., Taboureau, O., Hansen, K. B., Olsen, L., Egebjerg, J., Strømgaard, K., and Kristensen, A. S. (2009) Location of the antidepressant binding site in the serotonin transporter: importance of Ser-438 in recognition of citalopram and tricyclic antidepressants. *J. Biol. Chem.* **284**, 10276–10284

90.   Zhou, Z., Zhen, J., Karpowich, N. K., Goetz, R. M., Law, C. J., Reith, M. E. A., and Wang, D.-N. (2007) LeuT-desipramine structure reveals how antidepressants block neurotransmitter reuptake. *Science* **317**, 1390–3 [online] http://www.pubmedcentral.nih.gov/articlerender.fcgi?artid=3711652&tool=pmcentrez&rendertype=abstract

91.   Chen, N., Zhen, J., and Reith, M. E. A. (2004) Mutation of Trp84 and Asp313 of the dopamine transporter reveals similar mode of binding interaction for GBR12909 and benztropine as opposed to cocaine. *J. Neurochem.* **89**, 853–64 [online] http://www.ncbi.nlm.nih.gov/pubmed/15140185

92.   Kniazeff, J., Shi, L., Loland, C. J., Javitch, J. A., Weinstein, H., and Gether, U. (2008) An intracellular interaction network regulates conformational transitions in the dopamine transporter. *J. Biol. Chem.* **283**, 17691–701 [online] http://www.pubmedcentral.nih.gov/articlerender.fcgi?artid=2427322&tool=pmcentrez&rendertype=abstract

93.   Loland, C. J., Desai, R. I., Zou, M.-F., Cao, J., Grundt, P., Gerstbrein, K., Sitte, H. H., Newman, A. H., Katz, J. L., and Gether, U. (2008) Relationship between conformational changes in the dopamine transporter and cocaine-like subjective effects of uptake inhibitors. *Mol. Pharmacol.* **73**, 813–823

94.   Fedan, J. S. (1983) Pharmacological and biochemical applications of photoaffinity labels. Introduction. *Fed. Proc.* **42**, 2825 [online] http://www.ncbi.nlm.nih.gov/pubmed/6873310

95.   Dormán, G., and Prestwich, G. D. (2000) Using photolabile ligands in drug discovery and development. *Trends Biotechnol.* **18**, 64–77 [online] http://www.ncbi.nlm.nih.gov/pubmed/10652511

96.   Carroll, F. I., Gao, Y., Abraham, P., Lewin, A. H., Lew, R., Patel, A., Boja, J. W., and Kuhar, M. J. (1992) Probes for the cocaine receptor. Potentially irreversible ligands for the dopamine transporter. *J. Med. Chem.* **35**, 1813–1817

97.   Zou, M. F., Kopajtic, T., Katz, J. L., Wirtz, S., Justice, J. B., and Newman, A. H. (2001) Novel tropane-based irreversible ligands for the dopamine transporter. *J. Med. Chem.* **44**, 4453–61 [online] http://www.ncbi.nlm.nih.gov/pubmed/11728190

98.   Lever, J. R., Zou, M.-F., Parnas, M. L., Duval, R. A., Wirtz, S. E., Justice, J. B., Vaughan, R. A., and Newman, A. H. Radioiodinated azide and isothiocyanate derivatives of cocaine for irreversible labeling of dopamine transporters: synthesis and covalent binding studies. *Bioconjug. Chem.* **16**, 644–9 [online] http://www.ncbi.nlm.nih.gov/pubmed/15898733

99.   Newman, A. H., Cha, J. H., Cao, J., Kopajtic, T., Katz, J. L., Parnas, M. L., Vaughan, R., and Lever, J. R. (2006) Design and synthesis of a novel photoaffinity ligand for the dopamine and serotonin transporters based on 2beta-carbomethoxy-3beta-biphenyltropane. *J. Med. Chem.* **49**, 6621–5 [online] http://www.ncbi.nlm.nih.gov/pubmed/17064081

100.   Vaughan, R. a, Sakrikar, D. S., Parnas, M. L., Adkins, S., Foster, J. D., Duval, R. a, Lever, J. R., Kulkarni, S. S., and Hauck-Newman, A. (2007) Localization of cocaine analog [125I]RTI 82 irreversible binding to transmembrane domain 6 of the dopamine transporter. *J. Biol. Chem.* **282**, 8915–25 [online] http://www.ncbi.nlm.nih.gov/pubmed/17255098

101.   Parnas, M. L., Gaffaney, J. D., Zou, M. F., Lever, J. R., Newman, A. H., and Vaughan, R. A. (2008) Labeling of Dopamine Transporter Transmembrane Domain 1 Proximity of Cocaine and Substrate Active Sites. **73**, 1141–1150

102.   Konova, A. B., Moeller, S. J., Tomasi, D., Volkow, N. D., and Goldstein, R. Z. (2013) Effects of methylphenidate on resting-state functional connectivity of the mesocorticolimbic dopamine pathways in cocaine addiction. *JAMA psychiatry* **70**, 857–68 [online] http://archpsyc.jamanetwork.com/article.aspx?articleid=1699378

103.   Lapinsky, D. J., Velagaleti, R., Yarravarapu, N., Liu, Y., Huang, Y., Surratt, C. K., Lever, J. R., Foster, J. D., Acharya, R., Vaughan, R. A., and Deutsch, H. M. (2011) Azido-iodo-N-benzyl derivatives of threo-methylphenidate (Ritalin, Concerta): Rational design, synthesis, pharmacological evaluation, and dopamine transporter photoaffinity labeling. *Bioorg. Med. Chem.* **19**, 504–512 [online] http://www.ncbi.nlm.nih.gov/pubmed/21129986.

104. Lapinsky, D. J., Aggarwal, S., Nolan, T. L., Surratt, C. K., Lever, J. R., Acharya, R., Vaughan, R. a, Pandhare, A., and Blanton, M. P. (2012) (±)-2-(N-tert-Butylamino)-3'-[(125)I]-iodo-4'-azidopropiophenone: a dopamine transporter and nicotinic acetylcholine receptor photoaffinity ligand based on bupropion (Wellbutrin, Zyban). *Bioorg. Med. Chem. Lett.* **22**, 523–6 [online] http://www.pubmedcentral.nih.gov/articlerender.fcgi?artid=3249008&tool=pmcentrez&rendertype=abstract

105. Hastrup, H., Karlin, a, and Javitch, J. a (2001) Symmetrical dimer of the human dopamine transporter revealed by cross-linking Cys-306 at the extracellular end of the sixth transmembrane segment. *Proc. Natl. Acad. Sci. U. S. A.* **98**, 10055–10060 [online] http://www.pubmedcentral.nih.gov/articlerender.fcgi?artid=56914&tool=pmcentrez&rendertype=abstract.

106. Volz, T. J., and Schenk, J. O. (2005) A comprehensive atlas of the topography of functional groups of the dopamine transporter. *Synapse* **58**, 72–94 [online] http://www.ncbi.nlm.nih.gov/pubmed/16088952

107. Penmatsa, A., Wang, K. H., and Gouaux, E. (2013) X-ray structure of dopamine transporter elucidates antidepressant mechanism. *Nature* **advance on** [online] http://dx.doi.org/10.1038/nature12533

108. Vaughan, R. A., Gaffaney, J. D., Lever, J. R., Reith, M. E., and Dutta, A. K. (2001) Dual incorporation of photoaffinity ligands on dopamine transporters implicates proximity of labeled domains. *Mol. Pharmacol.* **59**, 1157–1164

109. Vaughan, R. A., and Kuhar, M. J. (1996) Dopamine transporter ligand binding domains. Structural and functional properties revealed by limited proteolysis. *J. Biol. Chem.* **271**, 21672–80 [online] http://www.ncbi.nlm.nih.gov/pubmed/8702957

110. Madras, B. K., Spealman, R. D., Fahey, M. A., Neumeyer, J. L., Saha, J. K., and Milius, R. A. (1989) Cocaine receptors labeled by [3H]2 beta-carbomethoxy-3 beta-(4-fluorophenyl)tropane. *Mol. Pharmacol.* **36**, 518–524

111. Boja, J. W., Carroll, F. I., Vaughan, R. A., Kopajtic, T., and Kuhar, M. J. (1998) Multiple binding sites for [125I]RTI-121 and other cocaine analogs in rat frontal cerebral cortex. *Synapse* **30**, 9–17

112. Missale, C., Castelletti, L., Govoni, S., Spano, P. F., Trabucchi, M., and Hanbauer, I. (1985) Dopamine uptake is differentially regulated in rat striatum and nucleus accumbens. *J. Neurochem.* **45**, 51–56

113. McElvain, J. S., and Schenk, J. O. (1992) A multisubstrate mechanism of striatal dopamine uptake and its inhibition by cocaine. *Biochem. Pharmacol.* **43**, 2189–2199

114. Bisgaard, H., Larsen, M. A. B., Mazier, S., Beuming, T., Newman, A. H., Weinstein, H., Shi, L., Loland, C. J., and Gether, U. (2011) The binding sites for benztropines and dopamine in the dopamine transporter overlap. *Neuropharmacology* **60**, 182–90 [online] http://www.ncbi.nlm.nih.gov/pubmed/20816875

115. Hill, E. R., Huang, X., Zhan, C.-G., Ivy Carroll, F., and Gu, H. H. (2011) Interaction of tyrosine 151 in norepinephrine transporter with the 2β group of cocaine analog RTI-113. *Neuropharmacology* **61**, 112–120

116. Merchant, B. A., and Madura, J. D. (2012) Insights from molecular dynamics: the binding site of cocaine in the dopamine transporter and permeation pathways of substrates in the leucine and dopamine transporters. *J. Mol. Graph. Model.* **38**, 1–12 [online] http://www.pubmedcentral.nih.gov/articlerender.fcgi?artid=3547672&tool=pmcentrez&rendertype=abstract

117. Schmitt, K. C., Rothman, R. B., and Reith, M. E. A. (2013) Nonclassical pharmacology of the dopamine transporter: atypical inhibitors, allosteric modulators, and partial substrates. *J. Pharmacol. Exp. Ther.* **346**, 2–10

118. Plenge, P., Shi, L., Beuming, T., Te, J., Newman, A. H., Weinstein, H., Gether, U., and Loland, C. J. (2012) Steric hindrance mutagenesis in the conserved extracellular vestibule impedes allosteric binding of antidepressants to the serotonin transporter. *J. Biol. Chem.* **287**, 39316–39326

119. Singh, S. K., Yamashita, A., and Gouaux, E. (2007) Antidepressant binding site in a bacterial homologue of neurotransmitter transporters. *Nature* **448**, 952–6 [online] http://www.ncbi.nlm.nih.gov/pubmed/17687333

120. Zhou, Z., Zhen, J., Karpowich, N. K., Law, C. J., Reith, M. E. A., and Wang, D.-N. (2009) Antidepressant specificity of serotonin transporter suggested by three LeuT-SSRI structures. *Nat. Struct. Mol. Biol.* **16**, 652–657

121. Indarte, M., Madura, J. D., and Surratt, C. K. (2008) Dopamine transporter comparative molecular modeling and binding site prediction using the LeuT(Aa) leucine transporter as a template. *Proteins* **70**, 1033–46 [online] http://www.ncbi.nlm.nih.gov/pubmed/17847094

122. Wang, H., Goehring, A., Wang, K. H., Penmatsa, A., Ressler, R., and Gouaux, E. (2013) Structural basis for action by diverse antidepressants on biogenic amine transporters. *Nature* **advance on** [online] http://dx.doi.org/10.1038/nature12648

123. Pramod, A. B., Foster, J., Carvelli, L., and Henry, L. K. (2013) SLC6 transporters: structure, function, regulation, disease association and therapeutics. *Mol. Aspects Med.* **34**, 197–219 [online] http://www.ncbi.nlm.nih.gov/pubmed/23506866

124. Plenge, P., Gether, U., and Rasmussen, S. G. (2007) Allosteric effects of R- and S-citalopram on the human 5-HT transporter: evidence for distinct high- and low-affinity binding sites. *Eur. J. Pharmacol.* **567**, 1–9

125. Singh, S. K. (2008) LeuT: a prokaryotic stepping stone on the way to a eukaryotic neurotransmitter transporter structure. *Channels (Austin).* **2**, 380–389

126. Krishnamurthy, H., and Gouaux, E. (2012) X-ray structures of LeuT in substrate-free outward-open and apo inward-open states. *Nature* **481**, 469–74 [online] http://www.pubmedcentral.nih.gov/articlerender.fcgi?artid=3306218&tool=pmcentrez&rendertype=abstract

127. Piscitelli, C. L., and Gouaux, E. (2012) Insights into transport mechanism from LeuT engineered to transport tryptophan. *EMBO J.* **31**, 228–235

128. Piscitelli, C. L., Krishnamurthy, H., and Gouaux, E. (2010) Neurotransmitter/sodium symporter orthologue LeuT has a single high-affinity substrate site. *Nature* **468**, 1129–1132

129. Wang, H., Elferich, J., and Gouaux, E. (2012) Structures of LeuT in bicelles define conformation and substrate binding in a membrane-like context. *Nat. Struct. Mol. Biol.* **19**, 212–219

130. Henry, L. K., Meiler, J., and Blakely, R. D. (2007) Bound to be different: neurotransmitter transporters meet their bacterial cousins. *Mol. Interv.* **7**, 306–309

131. Vaughan, R. A., Agoston, G. E., Lever, J. R., and Newman, A. H. (1999) Differential binding of tropane-based photoaffinity ligands on the dopamine transporter. *J. Neurosci.* **19**, 630–6 [online] http://www.ncbi.nlm.nih.gov/pubmed/9880583

132. Runyon, S. P., and Carroll, F. I. (2008) in *Dopamine Transporters, Chemistry, Biology and Pharmacology* pp. 125–169, John Wiley and Sons

133. Tanda, G., Newman, A. H., and Katz, J. L. (2009) in *Advances in Pharmacology* (S.J. Enna and Michael Williams, ed.) pp. 253–289, Academic Press

134. Tanda, G., Li, S. M., Mereu, M., Thomas, A. M., Ebbs, A. L., Chun, L. E., Tronci, V., Green, J. L., Zou, M.-F., Kopajtic, T. A., Newman, A. H., and Katz, J. L. (2013) Relations between stimulation of mesolimbic dopamine and place conditioning in rats produced by cocaine or drugs that are tolerant to dopamine transporter conformational change. *Psychopharmacology (Berl).* **229**, 307–21 [online] http://www.ncbi.nlm.nih.gov/pubmed/23612854

135. Schmitt, K. C., and Reith, M. E. A. (2011) The atypical stimulant and nootropic modafinil interacts with the dopamine transporter in a different manner than classical cocaine-like inhibitors. *PLoS One* **6**, e25790

136. Loland, C. J., Mereu, M., Okunola, O. M., Cao, J., Prisinzano, T. E., Mazier, S., Kopajtic, T., Shi, L., Katz, J. L., Tanda, G., and Newman, A. H. (2012) R-modafinil (armodafinil): a unique dopamine uptake inhibitor and potential medication for psychostimulant abuse. *Biol. Psychiatry* **72**, 405–413

137. Mereu, M., Bonci, A., Newman, A. H., and Tanda, G. (2013) The neurobiology of modafinil as an enhancer of cognitive performance and a potential treatment for substance use disorders. *Psychopharmacology (Berl).* **229**, 415–434